

A “torn bag mechanism” of small extracellular vesicle release via limiting membrane rupture of *en bloc* released amphisomes (amphiectosomes)

Reviewed Preprint

Published from the original preprint after peer review and assessment by eLife.

[About eLife's process](#)

Reviewed preprint version 1



March 28, 2024 (this version)

Posted to preprint server

February 1, 2024

Sent for peer review

January 30, 2024

Tamás Visnovitz , Dorina Lenzinger, Anna Koncz, Péter M Vizi, Tünde Bárkai, Krisztina V Vukman, Alicia Galinsoga, Krisztina Németh, Kelsey Fletcher, Zsolt I Komlósi, Péter Lőrincz, Gábor Valcz, Edit I Buzás 

Semmelweis University, Department of Genetics, Cell- and Immunobiology, Nagyváradi tér 4. 1089 Budapest, Hungary • ELTE Eötvös Loránd University, Department of Plant Physiology and Molecular Plant Biology, Pázmány Péter sétány 1/c, 1117 Budapest, Hungary • HUN-REN-SU Translational Extracellular Vesicle Research Group, Nagyváradi tér 4. 1089 Budapest, Hungary • ELTE Eötvös Loránd University, Department of Anatomy, Cell and Developmental Biology, Pázmány Péter sétány 1/c, 1117 Budapest, Hungary • Department of Image Analysis, 3DHISTECH Ltd, Budapest, Hungary • HCEMM-SU Extracellular Vesicle Research Group, Hungary, Nagyváradi tér 4. 1089 Budapest, Hungary

 https://en.wikipedia.org/wiki/Open_access

 Copyright information

Abstract

Recent studies showed an unexpected complexity of extracellular vesicle (EV) biogenesis pathways. We previously found evidence that human colorectal cancer cells *in vivo* release large multivesicular body-like structures *en bloc*. Here, we tested whether this large extracellular vesicle type is unique to colorectal cancer cells. We found that all cell types we studied (including different cell lines and cells in their original tissue environment) released multivesicular large EVs. We also demonstrated that upon spontaneous rupture of the limiting membrane of the multivesicular large EVs, their intraluminal vesicles (ILVs) escaped to the extracellular environment by a “torn bag mechanism”. We proved that the multivesicular large EVs were released by ectocytosis of amphisomes (hence, we termed them amphiectosomes). Both ILVs of amphiectosomes and small EVs separated from conditioned media were either exclusively CD63 or LC3B positive. According to our model, upon fusion of multivesicular bodies with autophagosomes, fragments of the autophagosomal inner membrane curl up to form LC3B positive ILVs of amphisomes, while CD63 positive small EVs are of multivesicular body origin. Our data suggest a novel common release mechanism for small EVs, distinct from the exocytosis of multivesicular bodies or amphisomes, as well as the small ectosome release pathway.

eLife assessment

The authors present evidence that small extracellular vesicles can be secreted from cells inside larger vesicles that they call amphisomes, which then tear to release their small vesicle contents. There are questions and concerns relating to the quality of the data and the *in vivo* significance of the observations. The findings are potentially **important** but the data are **incomplete** and the claims are only partially supported.

Introduction

Extracellular vesicles (EVs) are phospholipid bilayer enclosed structures^{1,2,3}, which have important roles in cellular homeostasis and intercellular communication. Exosomes have been defined as small (~ 50-200 nm) EVs (sEVs) of endosomal origin^{1,3}. Although autophagy is a major cellular homeostatic mechanism, and is implicated in a broad spectrum of human diseases, the intersection of autophagy and exosome secretion remains poorly understood. Recently, regulatory interactions have been shown between autophagy-related molecules and EV biogenesis^{4,5}. Furthermore, the LC3-conjugation machinery was demonstrated to specify the cargo packaged into EVs⁶. Importantly, both others and we reported the secretion of LC3-carrying exosomes^{6,7}. Particularly relevant to the findings presented here, is the implication of amphisomes (hybrid organelles formed by the fusion of late endosomes/multivesicular bodies (MVBs) with autophagosomes^{8,9}) in EV biogenesis. It was suggested that fusion of the limiting membrane of amphisomes with the plasma membrane of cells results in a subsequent release of exosomes by exocytosis^{1,3,10}. The current study was prompted by our recent data showing the *in vivo en bloc* release of large, MVB-like sEV clusters by human colorectal cancer cells¹¹. Here we investigated if this was a colorectal cancer cell-specific phenomenon. Unexpectedly, we found that it was a general, autophagy-related mechanism of sEV release that we designated as “torn bag mechanism”.

Results and Discussion

In this study, we analyzed *in situ* fixed, cultured cells with the released EVs preserved in their original microenvironment on a gelatin/fibronectin coated surface, and we detected large multivesicular EVs (MV-IEVs) in sections of different immersion fixed organs. We tested tumorous HT29, HepG2, and non-tumorous HEK293, HEK293T-PalmGFP, HL1 cell lines, as well as primary suspension type bone marrow derived mast cells (BMMCs). In addition, we studied ultrathin sections of mouse kidney and liver.

By the analysis of transmission electron micrographs of all tested cell types, we identified budding (Fig.1A-G) and secretion (Fig.1H-N) of MV-IEVs carrying intraluminal vesicles (ILVs). Importantly, in all cases we found evidence for the extracellular rupture of the limiting membrane of MV-IEVs and the release of ILVs (Fig.1O-U). For this novel type of sEV release, we suggest the designation “torn bag mechanism” which is distinct from the exocytosis of MVBs and amphisomes^{1,3,10} and from the release of plasma membrane derived small EV (sEVs) by ectocytosis¹².

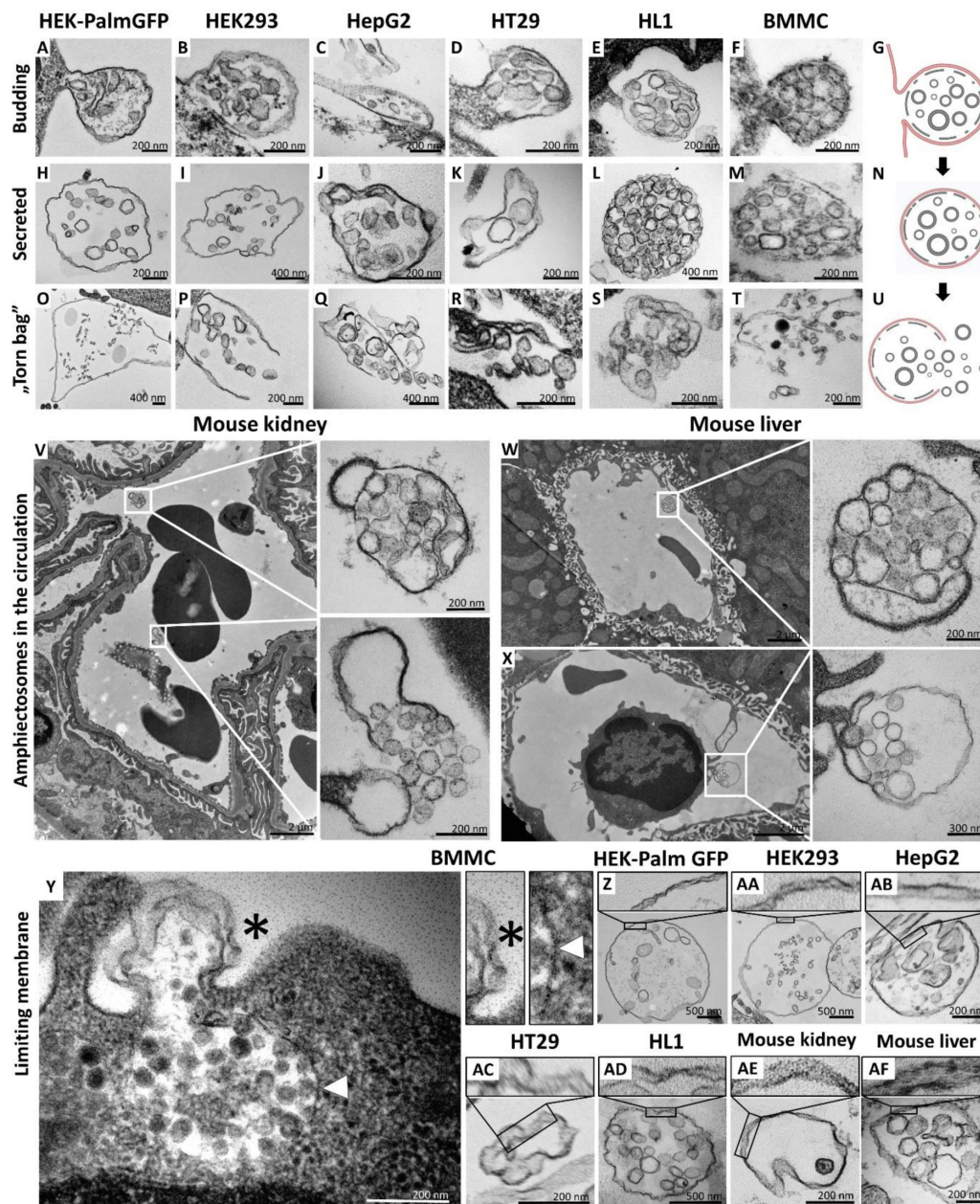


Figure 1.

Transmission electron microscopic detection of the release and extracellular fate of large, multivesicular EVs secreted by different cell lines and cells in mouse organs

Major steps of the release of large, multivesicular EVs were detected in the case of all tested cell lines including the immortal, non-tumorous HEK293T-PalmGFP (A,H,O), HEK293 (B,I,P), the tumorous cell lines HepG2 (C,J,Q) and HT29 (D,K,R), the beating cardiomyocyte cell line HL1 (E,L,S) and the primary suspension of bone marrow derived mast cells (BMMCs) (F,M,T). The different phases of EV secretion were also captured in the circulation of mouse kidney (V) and liver (W,X). According to the electron micrographs, we found evidence for the budding (A-G,X) and secretion (H-N,V,W) of the multivesicular large EVs (MV-EVs). We also detected the extracellular rupture of the limiting membrane of the released MV-EVs with the escape of the intraluminal vesicles (ILVs) by a "torn bag mechanism" (O-U,V). Although it is not always clear whether the secreted MV-EVs have a single or double limiting membrane, several micrographs suggest the presence of the double membrane (Y-AF) in the secreted MV-EVs. In the case of BMMCs (Y), the release phase of a multivesicular structure is captured. The bottom portion of this structure embedded in the cytoplasm is surrounded by a single membrane (white arrow head) while the upper (budding) portion is covered by double membrane (asterisk).

Most relevant to the *in vivo* conditions, we also observed the same phenomenon within the blood vessels of ultrathin sections of both murine kidney (**Fig.1V**) and liver (**Fig.1W,X**). In these cases, both the intact MV-IEVs (**Fig.1V-X**) and the “torn bag release” of sEVs (**Fig.1V**) were detected. **Fig.1X** shows that a circulating leukocyte releases MV-IEVs by ectocytosis.

Next, we decided to further investigate the subcellular origin of the ILVs within the secreted MV-IEVs. We analyzed the microenvironment of *in situ* fixed HEK293T-PalmGFP cells by confocal microscopy. The PalmGFP signal of HEK293T-PalmGFP cells principally associates with the plasma membrane¹³ (**Fig.2_S1C-E**). The green fluorescence helped us to identify the plasma membrane-derived limiting membrane of MV-IEVs. In agreement with our previous findings on HT29 colorectal cancer cells, within the MV-IEVs, we found CD63/ALIX (**Fig.2A,G**) CD81/ALIX (**Fig.2B,H**), CD63/TSG101 (**Fig.2C,I**) and CD81/TSG101 (**Fig.2D,J**) double positive ILVs or ILV clusters. In line with a recent finding¹², CD81 was present in the plasma membrane-derived limiting membrane (**Fig.2B,D,F**), while CD63 was only found inside the MV-IEVs (**Fig.2A,C,E**).

Next we studied the possible autophagy related aspects of the secreted MV-IEVs. ILVs were tested for the autophagy marker LC3B in parallel with CD63 and CD81. Although LC3B, CD63 and CD81 were all present in association with the ILVs (**Fig.2E,F**), the LC3B and CD63 (**Fig.2K**) and the LC3B and CD81 (**Fig.2L**) signals did not overlap. **Fig.2M** shows that while the known sEV markers (CD63, CD81, TSG101 and ALIX) strongly co-localized with each other, LC3B positivity hardly showed co-localization with CD63 or CD81. Immunocytochemistry results of HT29 and HepG2 cells further validated the findings obtained with the HEK293T-PalmGFP cells (**Fig.2_S2**). The ILVs of HEK293T-PalmGFP and HepG2 cell lines were Rab7 positive (**Fig.2_S1A,B**) suggesting a late endosomal origin. Western blot validation of the applied antibodies is summarized in **Fig.2_S3**. The sEV markers were also tested on separated sEVs of HEK293T-PalmGFP cells by transmission electron microscopy (TEM). **Fig.2P** confirms the typical sEV morphology. With TEM double immunogold labelling, using anti-LC3B and anti-CD63 antibodies simultaneously, we found distinct LC3B positive (**Fig.2Q**, **Fig.2_S5O**) and CD63 positive (**Fig.2R**, **Fig.2_S5O**) sEVs. Based on the analysis of TEM images, the diameters of unlabeled, and LC3B positive and negative sEVs were determined (**Fig.2S**). The LC3B positive sEVs had a significantly larger diameter as compared to the LC3B negative ones. The simultaneous presence of CD63, CD81, TSG101, ALIX and the autophagosome marker LC3B within the MV-IEVs (rather than on their limiting membrane) identified the extracellular MV-IEVs as *en bloc* released amphisomes.

The “torn bag mechanism” was also monitored by live cell SIM² super-resolution microscopy analysis of HEK293T-PalmGFP-LC3RFP cells (**Fig.2N,O**). The release of the LC3 positive red fluorescent signal was detected within a relatively short period of time (260 sec) (**Fig.2O**). We could rule out the possibility that rupture of the limiting membrane detected by TEM (**Fig.1O-T,V**) was a fixation artefact by showing the release of LC3 positive sEVs from amphiectosomes with live-cell imaging. Characterization of the in-house developed HEK293T-PalmGFP-LC3RFP cell line is shown in **Fig.2_S4**.

In the following step, we addressed the question whether LC3, associated with the ILVs of MV-IEVs, indeed reflected autophagy origin. We tested MVBs (**Fig.2_S5A,F,K**), autophagosomes (**Fig.2_S5B,G,L**), amphisomes (**Fig.2_S5C,H,M**), amphiectosomes (**Fig.2_S5D,I,N**) and isolated sEV fractions of the same cells (**Fig.2_S5E,J,O**). Using immune electron microscopy, as expected, we found CD63 single positivity in MVBs (**Fig.2_S5K**). In autophagosomes, the limiting phagophore membrane was LC3B positive, and CD63 positivity was also present (**Fig.2_S5L**). The limiting membrane of amphisomes was LC3B negative, and the internal membranous structures were either LC3B or CD63 positive (**Fig.2_S5M**). The same immunostaining was also observed in the ILVs of the released amphiectosomes (**Fig.2_S5N**). Importantly, the separated sEVs of HEK293T-PalmGFP cells were either LC3B or CD63 positive (**Fig.2_S5O**). Thus, we confirmed our confocal microscopy results at the ultrastructural level. Using immunogold TEM, we provided further evidence for the budding/ectocytosis mechanism of amphiectosome release (**Fig.2_S5P**).

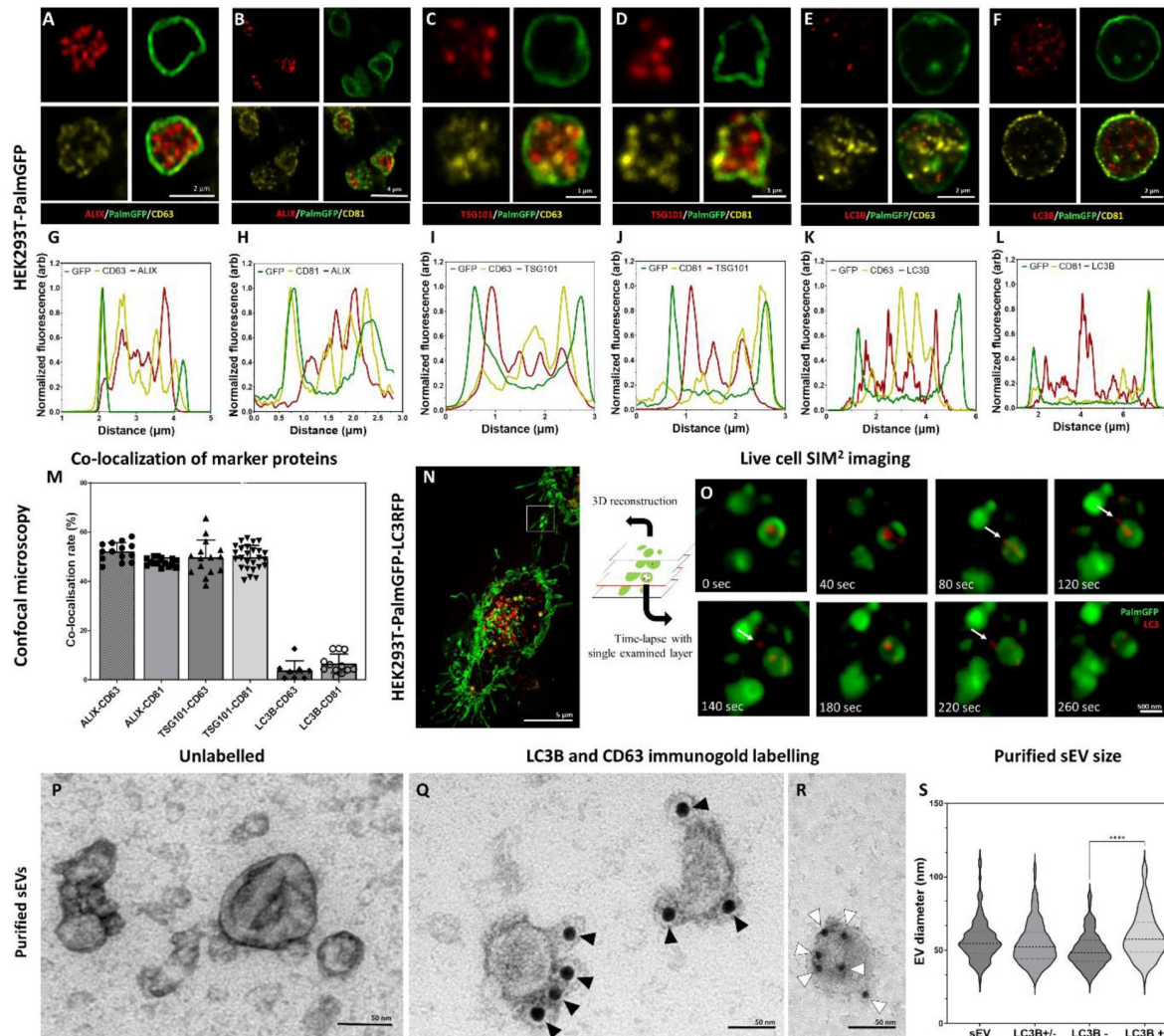


Figure 2.

Detection of conventional sEV markers and the LC3 protein in HEK293T-PalmGFP cell-derived EVs

Widely used sEV markers (CD63, CD81, ALIX and TSG101) and LC3B were tested in MV-IEVs found in the microenvironment of the releasing cells by confocal microscopy after *in situ* fixation (A-F). Normalized fluorescence intensities were calculated in order to determine the relative localization of the limiting membrane (PalmGFP), the conventional sEV markers and the LC3B signal (G-L). Fluorescence intensity peaks of sEV markers were largely overlapping with each other, while the LC3B signal and the sEV markers showed separation. Co-localization rates were also calculated (M). The sEV markers co-localized with one another as no significant difference was found among them. In contrast, low co-localization rates were detected between the “classical” sEV markers and LC3B (one-way ANOVA, $p < 0.0001$, $n = 8-26$ confocal images). Real time release of LC3 positive sEVs by the “torn bag mechanism” was studied in the case of HEK293T-PalmGFP-LC3RFP cells by Elyra7 SIM² super-resolution live cell imaging (N,O). Images were recorded continuously, and selected serial time points are shown. LC3 positive, red fluorescent small particles were released within a 5 min timeframe (O) and are indicated by white arrows. Presence of CD63 and LC3B were detected in the case of a separated sEV fraction using immunogold TEM. HEK293T-PalmGFP derived sEV fraction is shown by negative-positive contrast without immune labelling (P). In double-labelled immunogold TEM images (Q,R), distinct LC3B positive (Q) and CD63 positive (R) sEVs were found. However, CD63-LC3B double positive EVs were not detected. Black arrowheads indicate 10 nm gold particles identifying LC3B, while white arrowheads show 5 nm gold particles corresponding to the presence of CD63. Quantitative analysis of TEM images was performed (S), and the diameters of different EV populations were determined. The LC3B negative population was significantly smaller than the LC3B positive one ($p < 0.0001$, t-test; $n = 79-100$). No difference was detected when the immunogold labelled sEV fraction (either LC3B positive or negative, LC3B+/-) and the unlabeled sEV fraction (sEV) were compared ($p < 0.05$, t-test, $n = 112-179$).

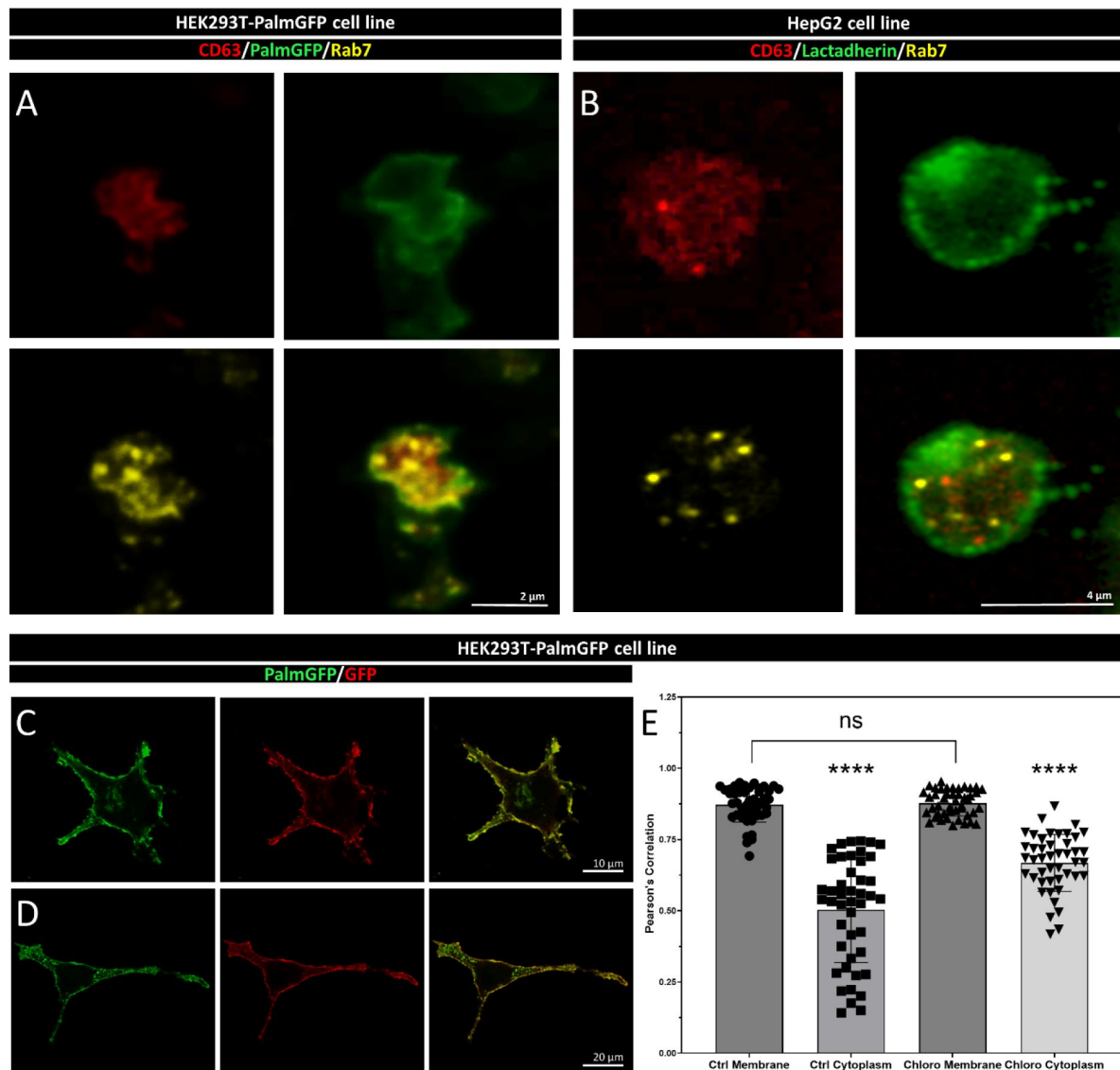


Fig.2_S1.

Confocal microscopic analysis of HEK293T-PalmGFP and HepG2 cells derived IEVs; HEK293T-PalmGFP cells

The MV-IEVs released by HEK293T-PalmGFP (A) and HepG2 cells (B) were tested for CD63 sEV and Rab7 late endosomal markers. Both CD63 and Rab7 were present in the ILVs. The GFP positivity of the HEK293T-PalmGFP cells was controlled by immunofluorescence microscopy on control (C) and Chloroquine-treated (D) cells. Co-localization of Palm-GFP and the anti-GFP signal was calculated in the plasma membrane and in the cytoplasm (E) and Pearson's correlations were visualized. The green fluorescence in the plasma membrane was clearly GFP-dependent in the case of control (Ctrl Membrane) and Chloroquine-treated (Choro Membrane) samples, while in the cytoplasm, the correlation was significantly weaker (Ctrl Cytoplasm and Choro Cytoplasm). Within the cytoplasm, the correlation was stronger in Chloroquine-treated cells, suggesting that the phagophore membrane may accumulate Palm-GFP ($p < 0.0001$, t-test; $n = 45$).

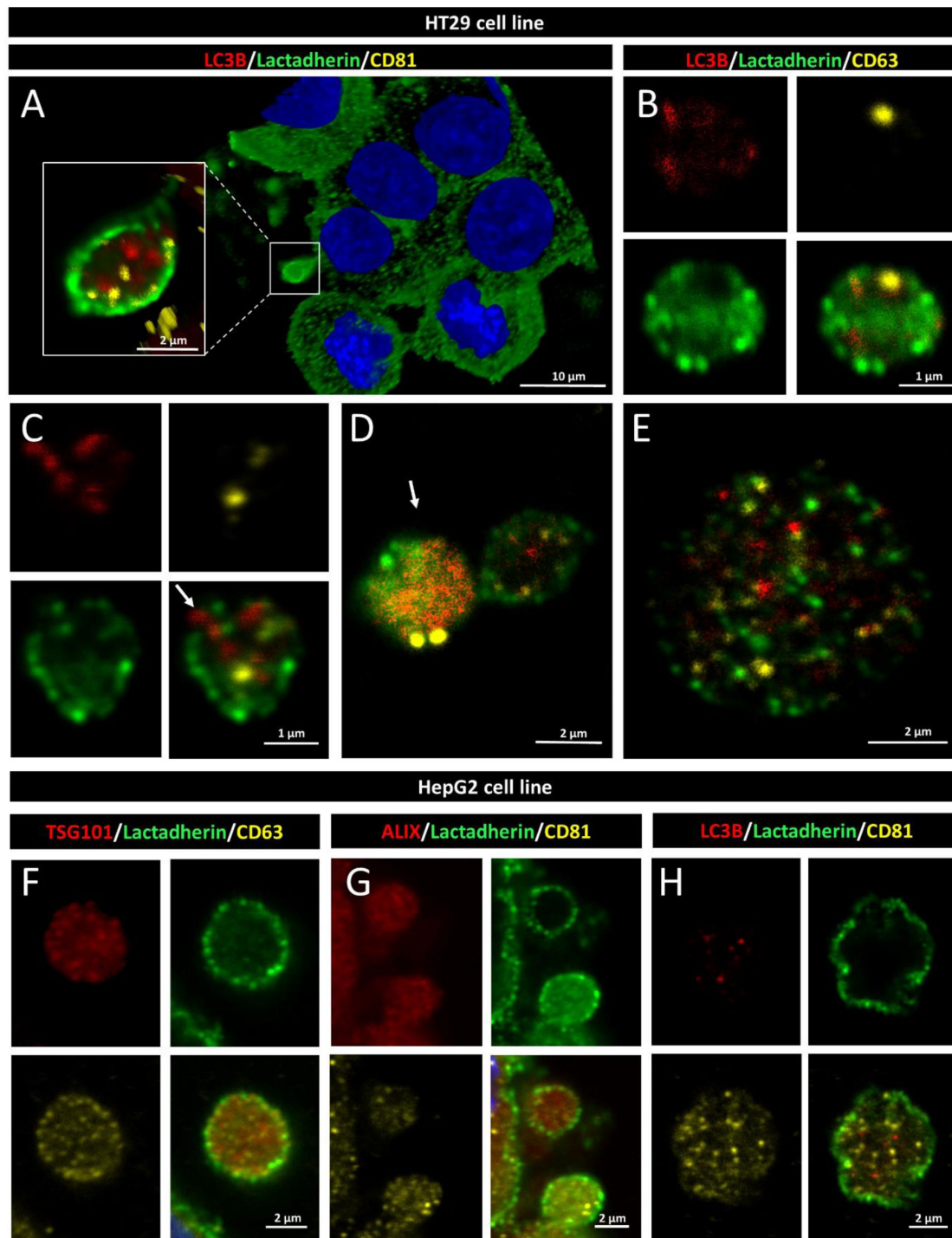


Fig.2_S2

Confocal microscopic images of amphictosome release by HT29 and HepG2 cells

The intraluminal EVs of amphictosomes were found to be positive for LC3B and CD81 in HT29 cultures (A) and HepG2 cells (H). In the case of HT29 cells, phases of the “torn bag mechanism” were captured, including a secreted intact amphictosome (B), MV-IEV with ruptured limiting membrane releasing internal vesicles (C, white arrow), an inside-out secreted amphictosome (D, white arrow), and an amphictosome with a fully disintegrated limiting membrane and released sEVs (E). The presence of TSG101/CD63 (F), ALIX/CD81 (G), and LC3B/CD81 (H) was also examined in the released amphictosomes of the HepG2 cell line.

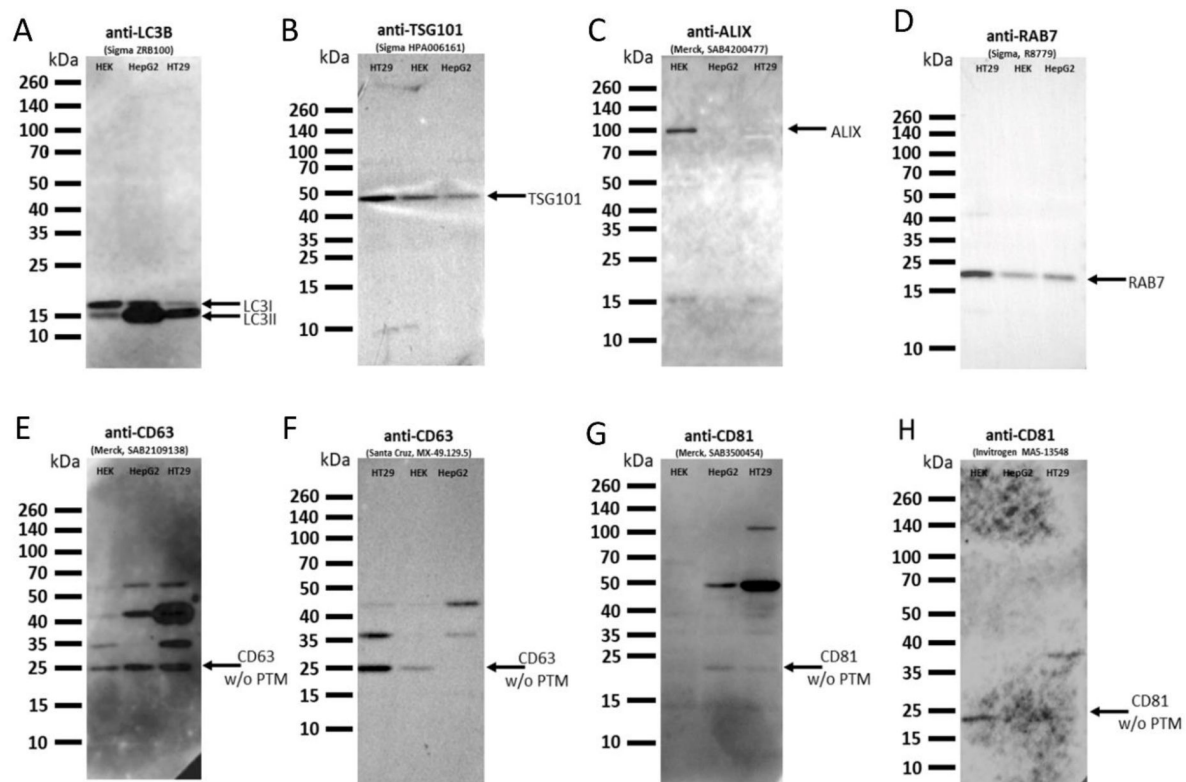


Fig.2_S3.

Western blot validation of antibodies used in immune-fluorescence detection

Lysates from three distinct human cell lines (HEK293, HepG2 and HT29) were employed in the validation process to reduce the cell line-specific variations in the study. Protein bands lacking posttranslational modifications are noted as "w/o PTM." Numerous posttranslational modifications of CD63 and CD81 are widely recognized.

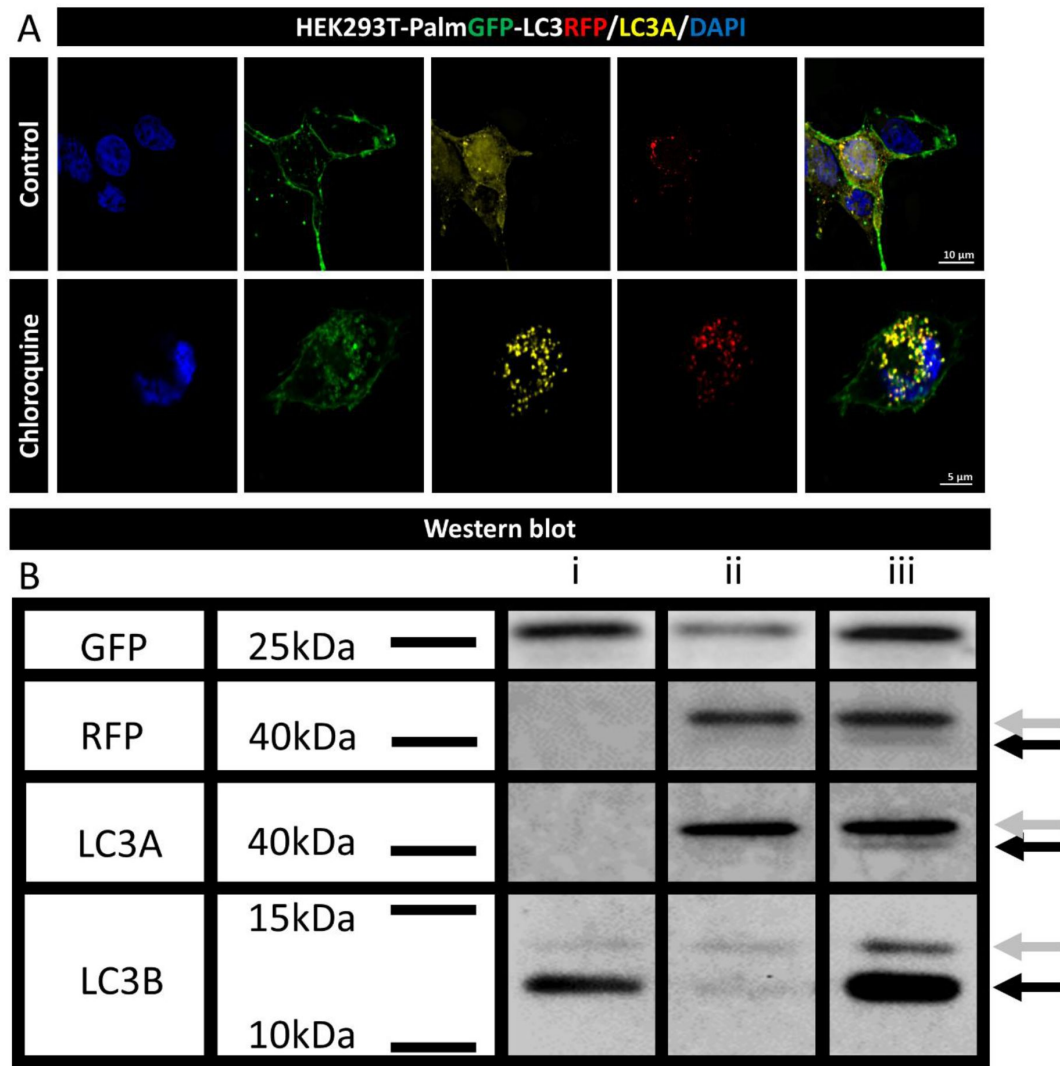


Fig.2_S4.

Characterization of the HEK293T-PalmGFP-LC3RFP cell line.

Confocal microscopy (A) and Western blot analysis (B) were employed to characterize the HEK293T-PalmGFP-LC3RFP cell line. For overnight Chloroquine treatments, 30 μ M Chloroquine was applied. Punctate LC3 fluorescence observed in (A) corresponds to autophagosomes. In panel (B), whole-cell lysates from HEK293T-PalmGFP (lane i), HEK293T-PalmGFP-LC3RFP (lane ii) and Chloroquine-treated HEK293T-PalmGFP-LC3RFP (lane iii) samples were examined. Gray arrows indicate LC3I, while black arrows highlight LC3II. Full Western Blot images can be found in [Fig.3_S2](#) supplementary figure.

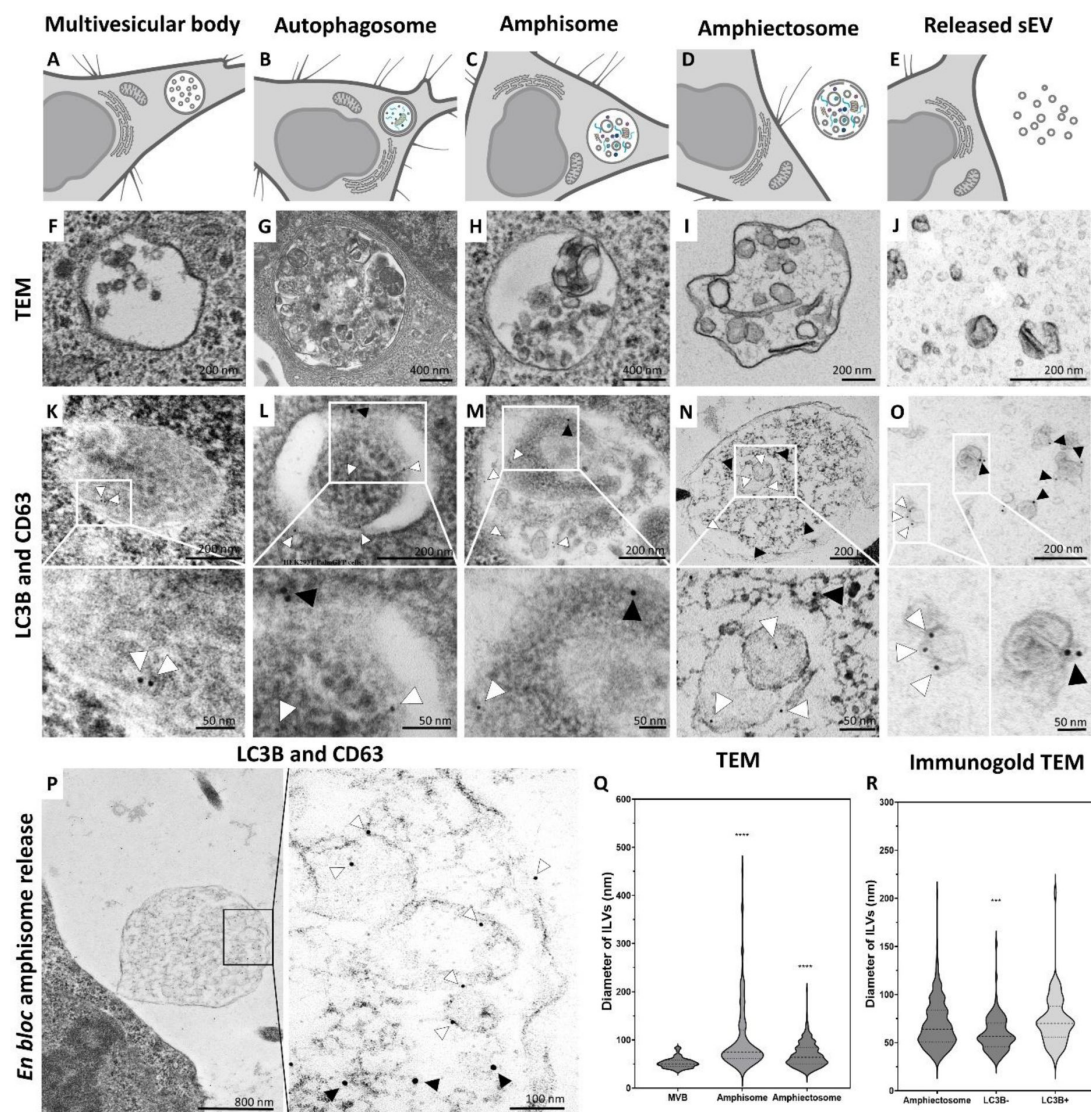


Fig.2_S5.

Structures involved in amphiectosome release

Multivesicular body (MVB, A), autophagosome (B), amphisome (C), amphiectosome (D) and secreted sEVs (E) were identified by TEM with and without immunogold labelling of HEK293T-PalmGFP cell cultures. White arrowheads (5 nm gold particles) indicate CD63 and black arrowheads (10 nm gold particles) show LC3B. While MVBs (F) were LC3B negative (K), we detected CD63 positivity on the surface of the ILVs (K). In an autophagosome (G), the limiting membrane layers were double positive for CD63 and LC3B (L). In contrast, the internal membranes of autophagosome were CD63 single positive (L). In the case of an amphisome (H), heterogeneous membrane structures were visible with variable size and morphology. The ILVs were either CD63 or LC3B positive (M). The amphiectosomes were located in the extracellular space and contained ILVs of different size and shape (I). The ILVs of amphiectosome (as in case of amphisome), were either CD63 or LC3B positive (N). Secreted sEVs (J) with immunogold labelling (O), were also found to be either CD63 or LC3B positive. Release of an amphiectosome is shown (P) with CD63 and LC3B immunogold signals. Higher magnification of the insert is indicated by the black rectangle. It shows either CD63 or LC3B positive ILVs. Size distributions of ILVs of MVBs, amphisomes and amphiectosomes were determined on Epon-embedded ultrathin sections (Q). Although the ILV sizes differed significantly (one-way ANOVA, ****: $p < 0.0001$, $n = 73$, 138 and 595, respectively), the majority of ILVs had a diameter between 40-100 nm. The diameter of LC3B positive and negative ILVs of amphiectosomes was assessed on TEM images of immunogold labelled ultrathin sections (R). LC3B negative ILVs were significantly smaller than the LC3B positive ones, while the ILVs in the Epon-embedded sections did not differ from the LC3B positive ones (one-way ANOVA, $p < 0.001$, $n = 595$, 101 and 70, respectively).

The diameters of ILVs within MVBs, amphisomes and amphiectosomes were compared (**Fig.2_S5Q**), and the differences were likely due to the different pH and osmotic conditions within these organelles. In agreement with our observations with separated sEVs, LC3B positive ILVs had a significantly larger diameter than the LC3B negative ones (**Fig.2_S5R**) possibly indicating their different intracellular origin. Based on all the above findings, we propose the following model (**Fig.3A**): autophagosomes and MVBs fuse to form amphisomes, and the inner, LC3 positive membrane of autophagosomes disintegrates¹⁴. It curls up and forms LC3 positive ILVs. Therefore, amphisomes contain both MVB-derived and autophagosome-derived, LC3 negative and positive ILVs, respectively. The amphisome is next released from the cell by ectocytosis. Finally, the plasma membrane-derived limiting membrane ruptures enabling the ILVs escape to the extracellular space by a “torn bag mechanism”.

To investigate the process of amphiectosome release, we exposed the MV-IEV releasing cells to different *in vitro* treatments (**Fig.3B**). The release of MV-IEVs was monitored by confocal microscopy of *in situ* fixed cell cultures. Optimal test conditions were determined (**Fig.3_S1A-F**) and the results are summarized in **Fig.3C**. Cytochalasin B did not have any effect on the discharge of MV-IEVs suggesting that the release did not involve a major actin-dependent mechanism. In contrast, there was a significant reduction of the MV-IEV secretion upon exposure of the cells to Colchicine indicating a role of microtubules in the release of the MV-IEVs. While Rapamycin significantly reduced the discharge of MV-IEVs, Chloroquine and Bafilomycin induced an enhanced MV-IEV secretion. Rapamycin activates autophagic degradation¹⁵, therefore, it induces a shift towards degradation as opposed to secretion. The lysosomotropic agents Chloroquine and Bafilomycin are known to interfere with the acidification of lysosomes^{16, 17}. By blocking the degradation pathway of MVBs/amphisomes (**Fig.3B**), an enhanced sEV secretion is observed. This effect is well known for exosome secretion from MVBs^{18, 19}. The diameters of the released MV-IEVs were determined based on confocal images (**Fig.3_S1G**). Metabolic activity of the cells was determined by a Resazurin assay, and a significant reduction was detected upon exposure of the cells to Rapamycin (**Fig.3_S1D**) in line with previously published data²⁰. LC3II is the membrane-associated, lipidated autophagic form of LC3²¹ and it is the hallmark of autophagy related membranes¹⁴. Importantly, by Western blot, we not only showed the presence of the membrane-bound LC3II in serum-free, IEV-depleted (sEV containing) conditioned medium of both HEK293T-PalmGFP and HEK293T-PalmGFP-LC3RFP cells, but the amount of LC3II substantially increased upon Chloroquine treatment (**Fig.3D**). Raw data of Western blots are available in **Fig.3_S2**.

Recent advances in the EV field shed light on migrasomes, a special type of MV-IEVs^{22, 23}. With their pomegranate-like ultrastructure, migrasomes resemble amphiectosomes. Therefore, we tested the presence of TSPAN4, a migrasome limiting membrane marker²³, in amphiectosomes. **Fig.4A,B,G,H** show that although TSPAN4 was present intraluminally in the HEK293T-PalmGFP-derived MV-IEVs, it was clearly absent from their limiting membrane. Surprisingly, we identified two different HT29 cell-derived MV-IEV populations: one with intraluminal TSPAN4 only (**Fig.4C,E,I,K**), and another one with a TSPAN4 positive limiting membrane (**Fig.4D,F,J,L**). This raised the possibility that the latter population corresponded to migrasomes. Our co-localization analysis also confirmed the existence of two distinct MV-IEV populations (**Fig.4M**). Next, we carried out live-cell imaging on HEK293T-PalmGFP-LC3RFP cells. The released MV-IEVs were either LC3 positive or negative intraluminally (**Fig.4N,O**). Our TEM images confirmed that certain cell types can release both migrasome-like structures and amphiectosomes. MV-IEVs with typical migrasome-associated retraction fiber(s) were detected in the case of HL1 (**Fig.4P**), HEK293T-PalmGFP (**Fig.4Q**) and BMMC cells (**Fig.4R**). Importantly, the same cells also released amphiectosomes by budding from the cell surface (**Fig.4S-U**). Taken together, based on the absence of TSPAN4 in their limiting membrane and their lack of association with retraction fibers, amphiectosomes appear to be distinct from migrasomes. Besides migrasomes, another MV-IEV type was described in the case of gastrointestinal tumors and low-grade glioblastoma cells referred to as spheresome^{24, 25}. However, there is no data on a relationship of spheresome

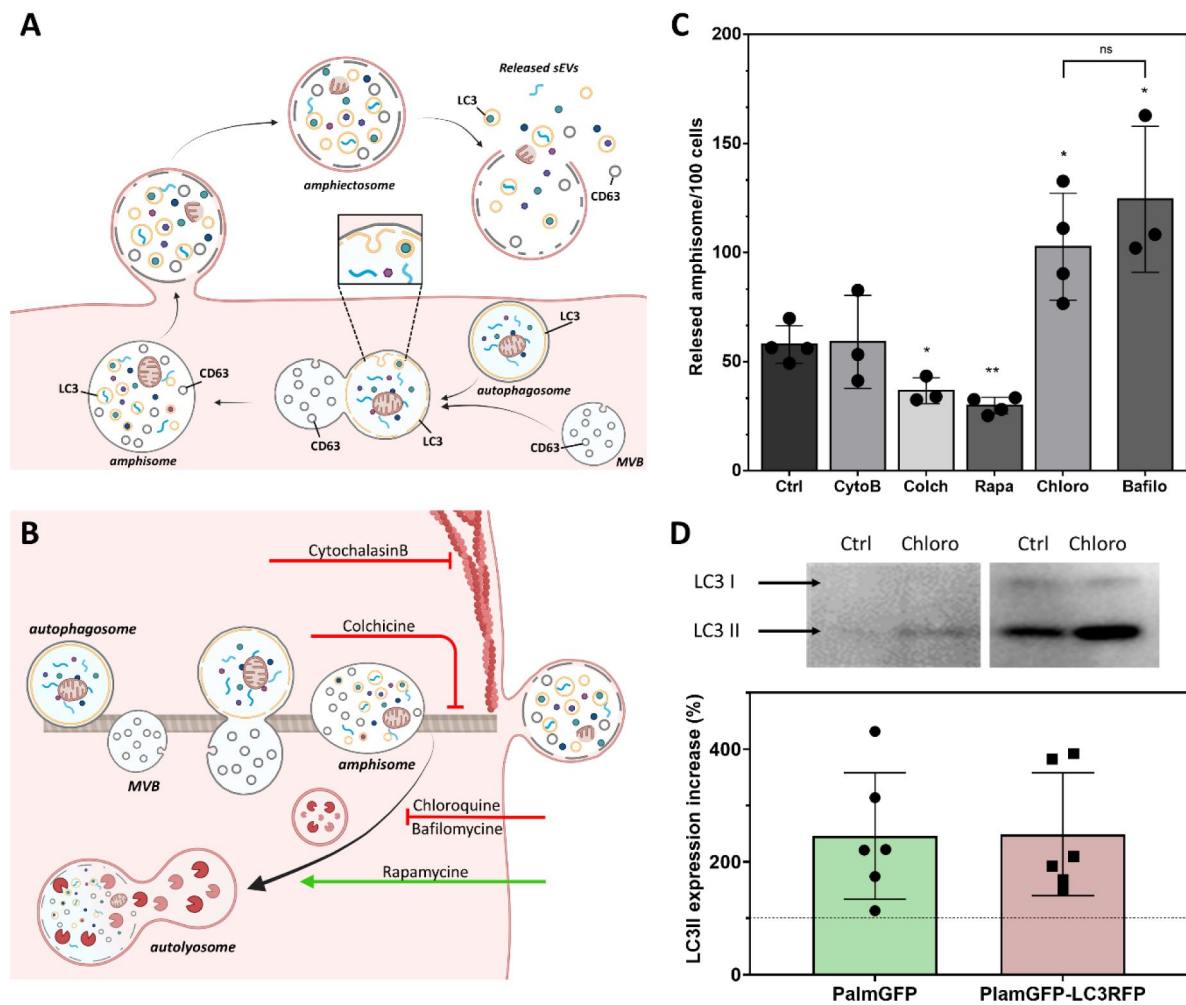


Figure 3.

Amphisome release and its modulation

Based on our data, a model of amphisome release was generated (A). According to this model, the fusion of MVBs and autophagosomes forms amphisomes. The LC3B positive membrane layer (indicated in orange) undergoes disintegration and forms LC3B positive ILVs inside the amphisome. Later, the amphisome is released into the extracellular space by ectocytosis and can be identified extracellularly as an amphiectosome. Finally, the limiting membrane(s) of the amphiectosome is ruptured and the ILVs are released as sEVs into the extracellular space by a “torn bag mechanism”. In order to further support our model on amphisome release and “torn bag” EV secretion different *in vitro* treatments were applied. Cytochalasin B, Colchicine, Chloroquine, Bafilomycin A1 and Rapamycin were used to modulate amphisome release. Points of actions are summarized (B). While Cytochalasin B inhibits actin-dependent membrane budding and cell migration, Colchicine blocks the microtubule-dependent intracellular trafficking. Chloroquine and Bafilomycin have similar, Rapamycin have opposite effects on lysosome-autophagosome or lysosome-amphisome fusion. Chloroquine and Bafilomycin inhibits lysosomal degradation while Rapamycin accelerates it. Based on confocal microscopy, Cytochalasin B (CytoB) did not alter the dynamics of amphisome release (C). In contrast, both Colchicine (Colch) and Rapamycin (Rapa) significantly inhibited the release of amphisomes, while Chloroquine (Chloro) and Bafilomycin (Bafilo) increased the release frequency. Between Chloroquine and Bafilomycin effect significant difference was not detected (C). Results are shown as mean \pm SD of 3-4 independent biological replicates, analyzed by one-way ANOVA, *: $p < 0.05$, **: $p < 0.01$, ns: non-significant. Presence of membrane-bound (lipidated) LC3II was tested by Western blotting. The total protein content of serum-, cell- and large EV-depleted conditioned medium of HEK293T-PalmGFP (PalmGFP) and HEK293T-PalmGFP-LC3RFP (PalmGFP-LC3RFP) cells was purified by precipitation and 20 μ g of the protein samples were loaded on the gel (D). The lipidated LC3II band was detected in all cases. Relative expression of control (Ctrl) and Chloro treated samples were determined by densitometry. Chloroquine treatment increased the LC3II level by approximately by two fold. Results are shown as mean \pm SD of $n=6$ biological replicates.

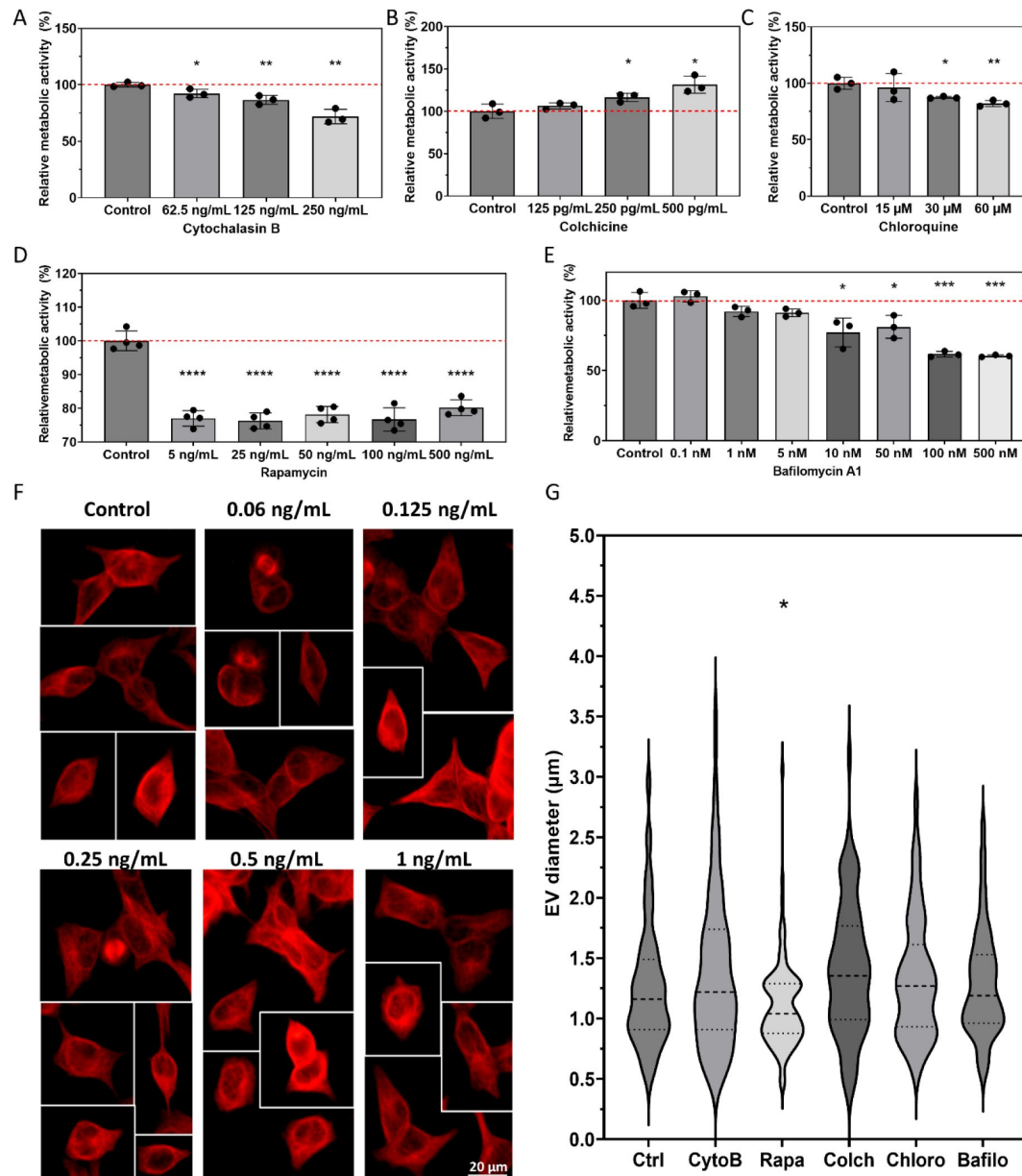


Fig.3 S1.

Dose determination for treatments and size distribution of MV-IEVs

Relative metabolic activity was assessed through a Resazurin assay (A-E) during treatment optimization. The red dashed line indicates 100 % metabolic activity, representing control cells. Results are presented as mean \pm SD values of $n=3-4$ independent biological replicates. Student's unpaired t-test was performed to compare control and treated cells (*: $p < 0.05$, **: $p < 0.01$, ****: $p < 0.0001$). For Colchicine treatment, alterations in the microtubular network were observed through immunocytochemistry (F) and documented using an epifluorescent microscope. Changes in the diameter of released amphitosomes under various treatments were determined on confocal microscopy images. A significant reduction in size was identified only in the case of Rapamycin treatment (G, one-way ANOVA test *: $p < 0.05$, $n = 95-101$).

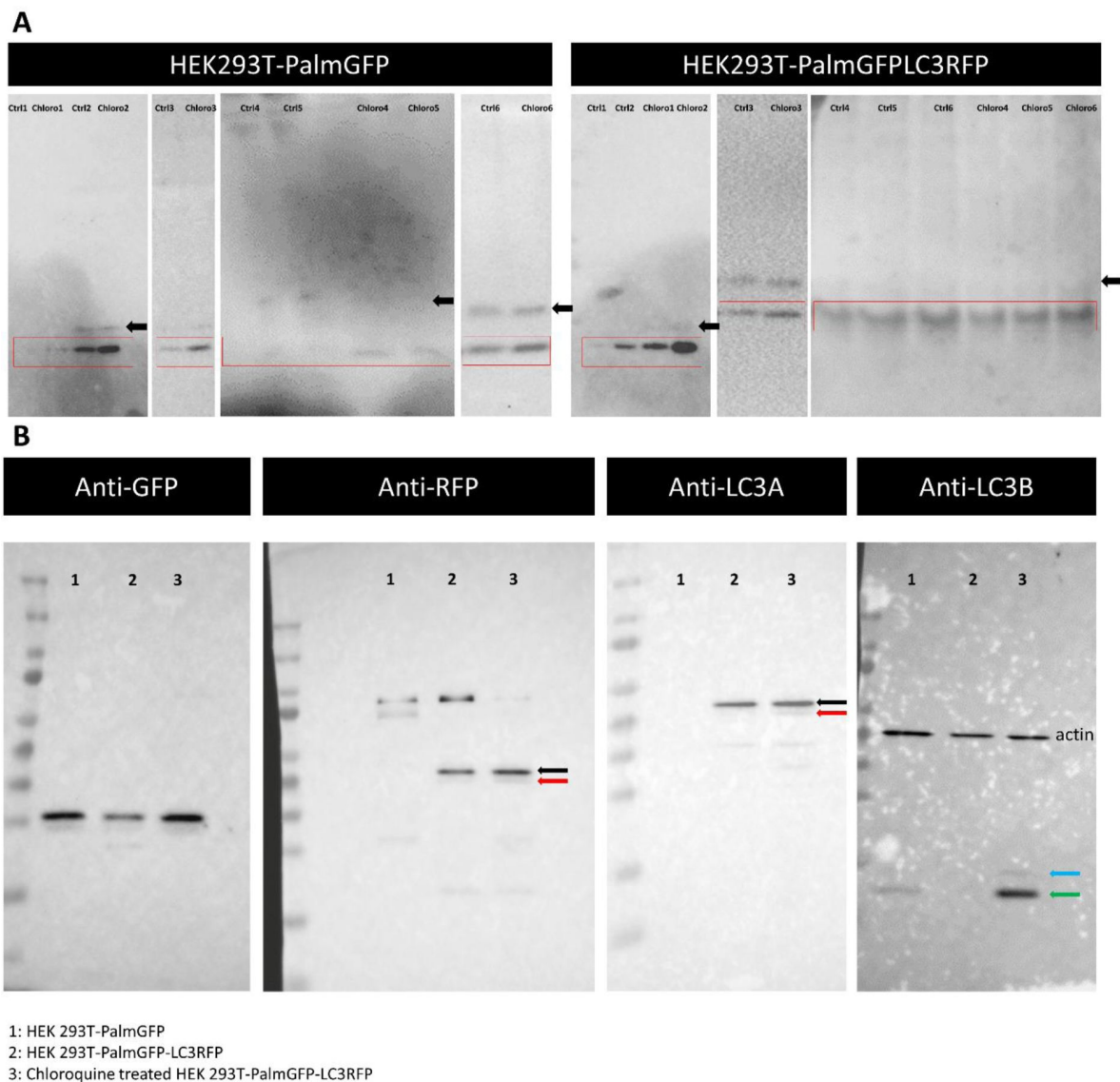


Fig.3_S2.

Unedited Western blots of Fig.2_S3 and Fig.3

Subfigure A displays the unedited Western blots utilized for the quantification in [Fig.3D](#). Black arrows indicate the location of LC3I, while red squares represent the quantified LC3II. In Subfigure B, the unedited blots from [Fig.2_S3B](#) are presented. Black arrows denote the LC3I-RFP fusion protein, while red arrows indicate the LC3II-RFP fusion protein. The blue arrow points to the native LC3I, while the green arrow represents the native LC3II protein.

release and autophagy. Recently, endothelial cell derived, multicompartmented microvesicles (MCMVs) were shown to protrude and pinch-off from the cell surface releasing ILVs by a mechanism similar to exocytosis²⁶[↗](#). The absence of protrusion clusters described for MCMV²⁶[↗](#) distinguishes amphiectosomes from MCMVs.

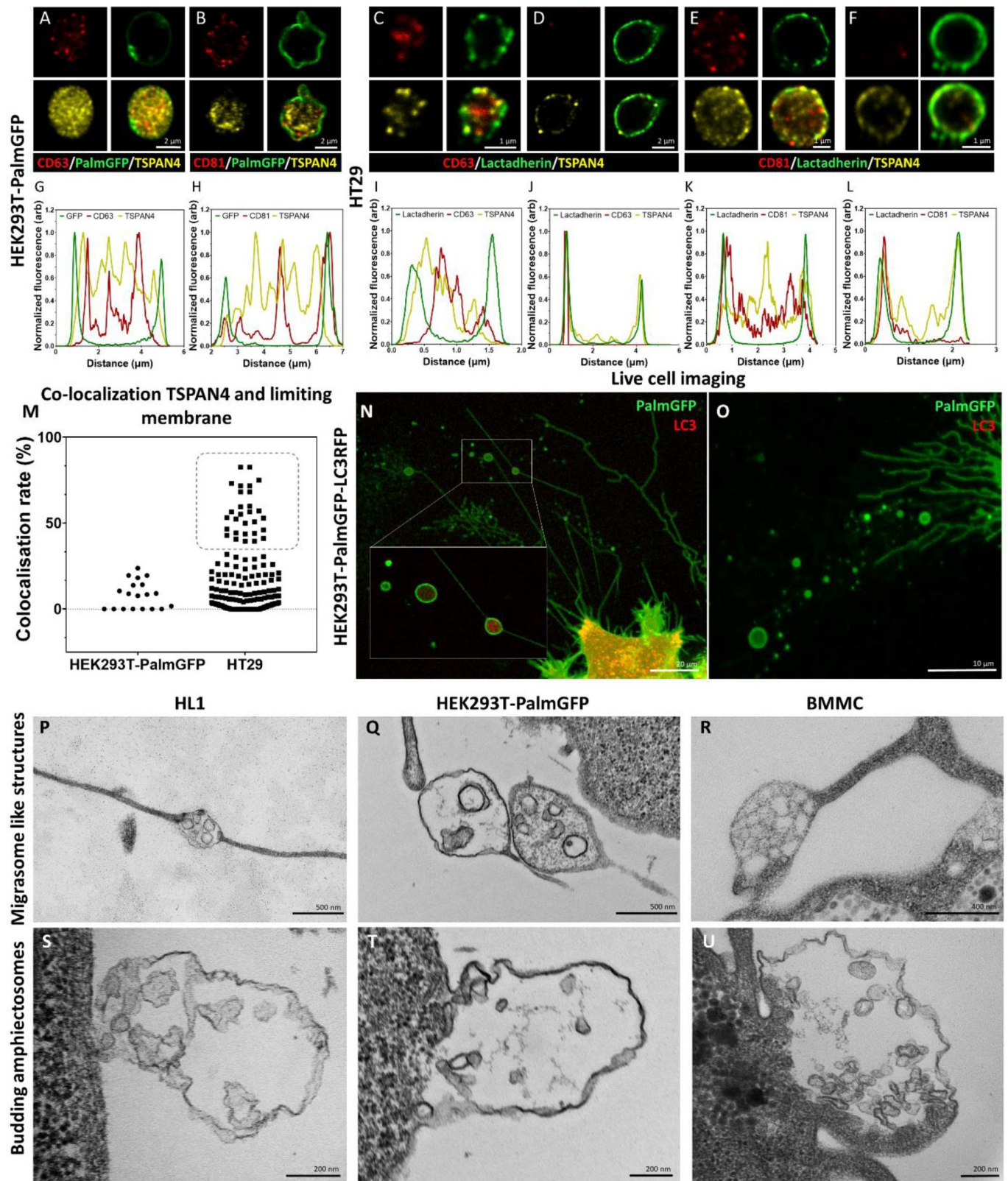


Figure 4.

Comparison of amphiectosomes and migrasomes

Commonly used sEV markers (CD63, CD81) and TSPAN4, a suggested migrasome marker, were tested in *in situ* fixed intact MV-IEVs of HEK293T-PalmGFP (A,B) and HT29 (C-F) cells by confocal microscopy. Normalized fluorescence intensities were calculated in order to determine the relative localization of the limiting membrane (with PalmGFP or lactadherin labelling) and the CD63/TSPAN4 and CD81/TSPAN4 markers (G-L). In the case of HEK293T-PalmGFP-derived EVs, there were no “classical migrasomes” with TSPAN4 in their limiting membrane were found. The TSPAN4 signal was only detected intraluminally in the MV-IEVs. The limiting membranes of HT29-derived MV-IEVs were either TSPAN4 positive and negative. The co-localization rate between the limiting membrane and TSPAN4 was low in case of HEK293T-PalmGFP-derived EVs. In the case of HT29 cells, two MV-IEV populations were identified: one with low and one with high co-localization rates (M). Live cell imaging of HEK293T-PalmGFP-LC3RFP cells showed migrasomes-like (retraction fiber-associated) MV-IEVs with or without intraluminal LC3 positivity (N,O). Using TEM, we could identify structures with retraction fiber-associated migrasome morphology in the case of HL1 (P), HEK293T-PalmGFP (Q) and BMMC (R) cells. For comparison, budding of amphiectosomes of the same HL1 (S), HEK293T-PalmGFP (T) and BMMC cells (U) are shown (without being associated with long retractions fibers).

Our approach, involving *in situ* fixation of cultures and tissues, made it possible to recognize sEV release from amphiectosomes by the “torn bag mechanism”. We propose that this mechanism can be easily missed if conditioned medium is subjected to centrifugation, SEC purification or even to simple pipetting, which may rupture of the limiting membrane of amphiectosomes. This aligns with our observation that the spontaneous escape of ILVs from untouched amphiectosomes can occur as early as 5 minutes after amphiectosome release. Our data presented here suggest that amphiectosome secretion and the “torn bag mechanism” may have a significant, however, previously unrecognized role in sEV biogenesis.

Material and methods

Key Resources Table				
Reagent type (species) or resource	Designation	Source or reference	Identifiers	Additional information
Cell line (<i>Homo sapiens</i>)	HEK293 human kidney(embryonic)	ECACC (Sigma)	#85120602	Batch No: 18E026
Cell line (<i>Homo sapiens</i>)	HT29 Caucasian colon adenocarcinoma grade II	ECACC (Sigma)	#91072201	Batch No 09K003
Cell line (<i>Homo sapiens</i>)	HepG2 human hepatocyte carcinoma	ECACC (Sigma)	#85011430	Batch No: 19B009
Cell line (<i>Mus musculus</i>)	HL1 mouse cardiomyocyte cell line, atrial	Merck	# SCC065	Batch No: RD1601001
Cell line (<i>Homo sapiens</i>)	HEK293T- PalmGFP human kidney(embryonic) expressing palmitoylated GFP	Kind gift of Charles Lai https://doi.org/10.1038/ncomms8029		Resorted before MCB preparation
Cell line (<i>Homo sapiens</i>)	HEK293T- PalmGFP- LC3RFP human kidney(embryonic) expressing palmitoylatedGFP and RFP tagged LC3	This paper		See material and methods
Cell line (<i>Mus musculus</i>)	BMMC bone marrow derived mast cells	Primary cell culture https://doi.org/10.1002/jev2.12023		
Lentiviral particles	LentiBrite RFP-LC3 Lentiviral Biosensor	Merck	17-10143	Batch No: 3530171

Biological sample (<i>Mus musculus</i>)	own animal house		C57BL/6	male, 12 weeks old
Antibody	rabbit polyclonal anti-CD63 (C- terminal)	Sigma/Merck	SAB2109138	IF (1:200) WB (1:500)
Antibody	mouse monoclonal anti-CD63	SantaCruz Biotechnology	MX-49.129.5 clone: sc-5275	IF (1:200) TEM (1:50) WB (1:1,000)
Antibody	rabbit polyclonal anti-CD81	Sigma/Merck	SAB3500454	IF (1:200) WB (1:2,500)
Antibody	mouse monoclonal anti-CD81	Invitrogen	MA5-13548 clone: 1.3.3.22	IF (1:100) WB (1:100)
Antibody	rabbit polyclonal anti-TSG101	Sigma/Merck	HPA006161	IF (1:200) WB (1:1,000)
Antibody	rabbit polyclonal anti-ALIX (C- terminal)	Sigma/Merck	SAB420047	IF (1:200) WB (1:1,000)
Antibody	rabbit monoclonal anti-LC3B	Sigma/Merck	ZRB100 clone: 12K5	IF (1:200) TEM (1:50) WB (1:1,000)
Antibody	rabbit monoclonal anti-LC3A	Sigma/Merck	ZRB1125 clone: 3J12	IF (1:200) WB (1:1,000)
Antibody	rabbit polyclonal anti-TSPAN4	Bioss	BS-9413R	IF (1:200)
Antibody	mouse monoclonal anti-Rab7	Sigma/Merck	R8779 clone: Rab7- 117	IF (1:200) WB (1:1,000)
Antibody	mouse monoclonal anti- α -tubulin	Sigma/Merck	T9026 clone: DM1A	IF (1:200)
Antibody	mouse monoclonal anti-GFP	Sigma/Merck	G6539 clone: GFP-20	IF (1:200) WB (1:1,000)
Antibody	mouse monoclonal anti-RFP	Invitrogen	MA5-15257 clone: RF5R	WB (1:1,000)
Antibody	goat anti- mouse IgG- ATTO550	Sigma/Merck	43394	IF (1:1,000)

Antibody	goat anti-rabbit IgG-ATTO647N	Sigma/Merck	40839	IF (1:1,000)
Antibody	goat polyclonal anti-rabbit IgG Fc (HRP)	abcam	ab97200	WB (1:10,000)
Antibody	goat polyclonal anti-mouse IgG Fc (HRP)	abcam	ab97265	WB (1:10,000)
Antibody	goat polyclonal anti-rabbit IgG (whole molecule) 10 nm gold pre-adsorbed	abcam	ab27234	TEM (1:50)
Antibody	goat polyclonal anti-mouse IgG (whole molecule) 5 nm gold pre-adsorbed	Sigma/Merck	G7527	TEM (1:50)
Chemical compound, drug	Bafilomycin A1	Sigma/Merck	B1793	Lot Number: 0000190389
Chemical compound, drug	Colchicine	Serva	77120.02	Lot Number: 190300
Chemical compound, drug	Chloroquine-diphosphate	Invitrogen	P36236 C	Lot Number: 2441325
Chemical compound, drug	Rapamycin	Sigma/Merck	R0395	Lot Number: 0000084976
Chemical compound, drug	Cytochalasin B	Sigma	C2743	Lot Number: 037M4083V
Chemical compound, drug	FBS	Biosera	FB-1090/500	Lot Number: 015BS575
Software, algorithm	LASX	Leica	Leica Application Suite X 3.5.5.19976	
Software, algorithm	ZEN Blue	Zeiss	ZEN 2.3 lite	
Software, algorithm	iTEM	Olympus	iTEM 5.1	

Software, algorithm	Image J	https://imagej.net/ij/	v1.54g	
Software, algorithm	Prism9	GraphPad	GraphPad Prism 9.4.1	
Software, algorithm	Biorender	https://www.biorender.com/		

Cell lines

The HEK293 human embryonic kidney, the HepG2 human hepatocyte carcinoma cell line and the HT29 human colon adenocarcinoma cell lines were purchased from the European Collection of Authenticated Cell Cultures (ECACC) through their distributor (Sigma). The HL1 cell line was purchased from Millipore. The HEK293T-PalmGFP human embryonic kidney cells was kindly provided by Charles P. Lai²⁷. Mouse bone marrow-derived mast cells (BMMCs) were differentiated and expanded as we described previously²⁸. The HEK293, HEK293T-PalmGFP and HepG2 cell lines were grown in DMEM (Gibco)^{29, 30}, the HT29 cells were cultured in RPMI 1640 (Gibco)¹¹, while the HL1 cells were grown in Claycomb medium³¹. All cells were cultured with 10 % fetal bovine serum (FBS, BioSera) in the presence of 100 U/mL of Penicillin and 100 µg/mL Streptomycin (Sigma).

Before analysis by confocal microscopy, the cells were cultured on the surface of gelatin-fibronectin coated glass coverslips (VWR). The coating solution contained 0.02 % gelatin (Sigma) and 5 mg/mL fibronectin (Invitrogen). Coverslips were coated overnight (O/N) at 37 °C.

For transmission electron microscopy (TEM), the adherent cells (HEK293, HEK293T-PalmGFP, HepG2, HT29 and HL1) were grown in gelatin-fibronectin coated 8-well Flux Cell Culture Slides (SPL).

Cell cultures were tested regularly for Mycoplasma infection by PCR, with the following PCR primers: GAAGAWATGCCWTATTTAGAAGATGG and CCRTTTTGACTYTTWCCAC-CMAGTGGTTGTG³¹.

Generation of HEK293T-PalmGFP-LC3RFP cell line

For generation of a stable HEK293T-PalmGFP-LC3RFP cell line, HEK293T-PalmGFP cells were transfected by LentiBrite RFP-LC3 Lentiviral particles (Merck) according to the instructions of the manufacturer. The GFP-RFP double positive cells were sorted by a HS800 Cell Sorter (SONY) and cell banks (master and working cell banks) were prepared. The success of the stable transfection was analyzed by immunocytochemistry and Western blotting. Results are shown in **Fig.2_S3**.

Confocal microscopy

Confocal microscopy was carried out as we described earlier^{28, 31} with some modifications. Briefly, unlike the majority of the studies in the field of EVs, here we analyzed untouched, *in situ* fixed and cultured cells and their microenvironment. Since centrifugation may disrupt the limiting membrane of amphiectosomes, the *in situ* fixation made it possible to observe them in their intact form. The culture medium was gently removed by pipetting from above the cells leaving a thin medium layer only (approximately 150 µL of liquid on the cells). Without any further washing, cells were *in situ* fixed by 4 % paraformaldehyde (PFA) in phosphate buffer saline (PBS) for 20 min at room temperature (RT). The released IEVs were either fixed and captured during the release or were preserved on the gelatin/fibronectin surface coating. After fixation, 3x 5 min washes with 50 mM glycine in PBS were carried out. In the case of the non-fluorescent HepG2 and HT29 cells, a lactadherin-based plasma membrane staining was performed^{13, 28, 31}.

Lactadherin (Haematologic Technologies) was conjugated to ATTO488 fluorophore (abcam) according to the instructions of the manufacturer. The lactadherin-ATTO488 conjugate was added to the cells in 1:100 dilution in PBS (for 1 h, RT). The unbound lactadherin was removed by washing with PBS (3 times, 5 min, RT) and post-fixation was carried out by 4 % PFA (20 min, RT). PFA was removed by washes with 50 mM glycine in PBS (3 times, 5 min, RT). Blocking and permeabilization of the cells were performed by 10 % FBS with 0.1 % TritonX-100 (Sigma) in PBS (1 h, RT). In general, primary antibodies were applied in 1:200 dilution O/N at 4 °C in the above blocking and permeabilization solution. Excess primary antibodies were eliminated by washing with the blocking and permeabilization solution (3 times, 5 min RT). The secondary antibodies were applied in 1:1000 dilution in 1 % FBS in PBS (1 h, RT). Unbound secondary antibodies were eliminated by washing (1 % FBS, in PBS, 2 times, 5 min; PBS 2 times, 5 min; water 2 times, 5 min) and the samples were mounted in ProLong Diamond with DAPI (Invitrogen). Slides were examined by Leica SP8 Lightning confocal microscope with adaptive lightning mode using a HC PL APO CS2 63x/1.40 OIL objective with hybrid detector. The applied lookup tables (LUT) were linear during this study. For image analysis and co-localization studies, we applied Leica LASX software using the unprocessed raw images. In case of co-localization studies, 20 % threshold and 10 % background settings were applied.

Transmission electron microscopy

Adherent cells (HEK293, HEK293T-PalmGFP, HepG2, HT29 and HL1), as well as mouse (C57BL/6) kidney and liver tissues pieces (approx. 1.5 mm x 1.5 mm) were immersed in and fixed by 4 % glutaraldehyde (48 h/4 °C), post-fixed by 1% osmium tetroxide (2 h, RT) and were embedded into Epon resin (Electron Microscopy Sciences) as described previously³². In the case of BMMCs, 920 µL cell suspension was complemented with 80 µL 50% glutaraldehyde to reach the final 4 % glutaraldehyde concentration. Cells were fixed for 48h at 4°C and were post-fixed by 1% osmium tetroxide (2 h, RT). During sample preparation, BMMCs were collected by gravity-based sedimentation. Due to the high viscosity of Epon resin, BMMCs were embedded in LR White low viscosity resin (SPI Supplies) according to the instructions of the manufacturer. Ultrathin sections (60 nm) were contrasted by uranyl acetate (3.75 %, 10 min, RT) and lead citrate (12 min, RT).

For immunogold TEM studies, cells and tissues were fixed by 4 % PFA with 0.1% glutaraldehyde (48 h, 4 °C) and were post-fixed by 0.5 % osmium tetroxide (30 min, RT). Samples were embedded into LR White and were immunogold labelled as described previously¹¹. The contrast was enhanced by uranyl acetate (3.75 %, 1 min, RT) and lead citrate (2 min, RT). Purified HEK293T-PalmGFP-derived sEV-s were detected by negative-positive contrasting and immunogold labelling as described previously³¹. Antibodies were used in 1:50 dilution. Detailed list of the used antibodies is available in the Key Resources Table.

For all electron microscopic studies, a JEOL 1011 transmission electron microscope was used. Images were captured with the help of Olympus iTEM software and for image analysis, Image J software was used.

Live cell imaging

The HEK293T-PalmGFP-LC3RFP stable cell line was cultured the same way as HEK293T-PalmGFP cells. Before the experiments, gelatin-fibronectin coated 10-well coverslip bottom chamber slide (Greiner-BioOne) was seeded and treated by 30 µM Chloroquine O/N. Release of migrasomes, amphiectosomes and sEVs were followed by the Leica SP8 Lightning confocal microscope equipped with an Okolab environmental chamber and a Zeiss ELYRA 7 with Lattice SIM² super-resolution fluorescent microscope with the help of 63x/1.4 plan-apochromat Oil objective. For image analysis, we applied Leica LASX, Zeiss ZEN Blue and Image J software.

Modulation of amphiectosome release

In order to test the release mechanism of amphiectosomes and to distinguish them from migrasomes, different treatments were applied overnight (O/N) in fresh, serum containing cell culture medium except for Colchicine, where 1 h treatment was selected. Maturation and fusion of endosomes and lysosomes were inhibited by 15.5 µg/mL (30 µM) Chloroquine (Invitrogen) and 10 nM BafilomycinA1 (Sigma). Actin polymerization was inhibited by 125 ng/mL Cytochalasin B (Sigma). Tubulin polymerization and function were inhibited by 250 pg/mL Colchicine, while an autophagy-related degradation was induced by 50 ng/mL Rapamycin. The selected concentrations were determined based both on literature data and our preliminary experiments ([Fig.3_S1](#)). Cellular metabolic activity was determined by a metabolic activity-based Resazurin assay³¹. Fresh cell culture medium was added to control cultures a day before the *in situ* fixation. Reagents were diluted in fresh cell culture medium. Leica TCS SP8 Lightning confocal microscope was used for detection of amphiectosome release. A few hundred µm² sized area with 15-20 µm in height was tile-scanned with a few hundred cells. The MV-LEVs were recognized as CD63 positive EVs surrounded by GFP positive membrane. They were counted and were normalized to the number of nuclei.

Western blotting

Presence of proteins and specificity of the used primary antibodies were confirmed by Western blotting as described previously³¹. For accurate quantification (free of variations potentially caused by EV purification), we analyzed cell-, serum- and LEV-free conditioned medium. The cells were cultured O/N in a serum-free culture medium. After harvesting, the cells were eliminated by centrifugation (300 g, 10 min at 4 °C) followed by a 2.000g centrifugation (30 min at 4 °C) to eliminate LEVs. Total protein content of the conditioned, serum-, cell- and LEV-free medium was precipitated by trichloroacetic acid as described previously^{31, 33}. The protein pellets were suspended in cOmplete Protease Inhibitor Cocktail (Roche) containing radio-immunoprecipitation assay (RIPA) buffer.

When whole cell lysate was tested for validation of antibodies and the HEK293T-PalmGFP-LC3RFP cell line, cells were lysed in cOmplete Protease Inhibitor Cocktail (Roche) containing RIPA buffer.

Polyacrylamide gel electrophoresis was carried out using 10 % gels (acrylamide/bis-acrylamide ratio 37.5:1) or any kDa precast gels (Biorad) and a MiniProtean (BioRad) gel running system. For better solubilization of membrane proteins, equal volumes of 0.1 % TritonX-100, Laemmli buffer and samples were mixed as described previously³⁴. Approximately 10-30 µg protein were loaded into each well. Following electrophoretic separation, proteins were transferred to PVDF membranes (Serva). Membranes were blocked with 5 % skimmed milk powder or 5 % BSA in washing buffer for 1 h. Primary antibodies were applied in 1:1000 dilution with the exception of the anti-CD63 (rabbit), anti-CD81 (rabbit) and anti-CD81 (mouse) antibodies where 1:500, 1:2500 and 1:100 dilutions were used, respectively. Peroxidase-labelled secondary antibodies were applied in 1:10 000 dilution. The signals were detected by ECL Western Blotting Substrate (Thermo Scientific) with an Imager CHEMI Premium (VWR) image analyzer system. In case of quantification, equal protein amounts were loaded to the gels. Within a biological replicate, the control and Chloroquine-treated samples were run on the same gels. To enable comparison, the relative expression of control and Chloroquine-treated samples were determined and compared.

Software and statistical analysis

For image capturing, analysis and co-localization studies, Leica LAS X, Zeiss ZEN Blue, Olympus iTEM and Image J software were used. Figures and graphs were generated using GraphPad Prism 9.4.1 and Biorender ([BioRender.com](#)). For statistical analysis, standard deviation was calculated. Unpaired two tailed student t-tests and one-way ANOVA were used (* p<0.05, ** p<0.01, *** p<0.001, **** p<0.0001).

Acknowledgements

This research was funded by the NVKP_16-1-2016-0004 grant of the Hungarian National Research, Development and Innovation Office (NKFIH), ÚNKP-23-3-I-SE-2, the Semmelweis Innovation Fund (STIA 2020 KFI), Hungarian Scientific Research Fund (OTKA K120237 and FK 138851), Eötvös Loránd University Excellence Fund (EKA 2022/045-P101), Hungary Academy of Sciences, LP2022-13/2022, VEKOP-2.3.2-16-2016-00002, VEKOP-2.3.3-15-2017-00016, the Higher Education Excellence Program (FIKP) and the Therapeutic Thematic Programme TKP2021-EGA-23. This study was also supported by the grants RRF-2.3.1-21-2022-00003 (National Cardiovascular Laboratory Program) and 2019-2.1.7-ERA-NET-2021-00015. The project has received funding from the EU's Horizon 2020 Research and Innovation Programme under grant agreement No. 739593.

The authors would like to thank Gábor Valcz for his invaluable support throughout the research process, for critically reviewing the manuscript and for his insightful comments. The authors would like to thank the ZEISS Microscopy Customer Center Team for the collaboration, and Dr. Abel Pereira da Graça for the possibility to use the Elyra7 SIM² super-resolution microscope. The authors are grateful to Györgyné Vidra, Györgyi Balogh and Andrea Orbán for their technical help and advises.

Conflict of interest

EIB is a member of the Advisory Board of Sphere Gene Therapeutics Inc. (Boston, MA, USA) and ReNeuron (UK).

References

- 1 Buzas E. I (2023) **The roles of extracellular vesicles in the immune system** *Nat Rev Immunol* **23**:236–250 <https://doi.org/10.1038/s41577-022-00763-8>
- 2 György B., et al. (2011) **Membrane vesicles, current state-of-the-art: emerging role of extracellular vesicles** *Cellular and Molecular Life Sciences* **68**:2667–2688 <https://doi.org/10.1007/s00018-011-0689-3>
- 3 Théry C., et al. (2018) **Minimal information for studies of extracellular vesicles 2018 (MISEV2018): a position statement of the International Society for Extracellular Vesicles and update of the MISEV2014 guidelines** *Journal of Extracellular Vesicles* **7** <https://doi.org/10.1080/20013078.2018.1535750>
- 4 Murrow L., Malhotra R., Debnath J (2015) **ATG12–ATG3 interacts with Alix to promote basal autophagic flux and late endosome function** *Nature Cell Biology* **17**:300–310 <https://doi.org/10.1038/ncb3112>
- 5 Guo H., et al. (2017) **Atg5 Disassociates the V1V0-ATPase to Promote Exosome Production and Tumor Metastasis Independent of Canonical Macroautophagy** *Developmental Cell* **43**:716–730 <https://doi.org/10.1016/j.devcel.2017.11.018>
- 6 Leidal A. M., et al. (2020) **The LC3-conjugation machinery specifies the loading of RNA-binding proteins into extracellular vesicles** *Nature Cell Biology* **22**:187–199 <https://doi.org/10.1038/s41556-019-0450-y>
- 7 Minakaki G., et al. (2018) **Autophagy inhibition promotes SNCA/alpha-synuclein release and transfer via extracellular vesicles with a hybrid autophagosome-exosome-like phenotype** *Autophagy* **14**:98–119 <https://doi.org/10.1080/15548627.2017.1395992>
- 8 Berg T. O., Fengsrud M., Strømhaug P. E., Berg T., Seglen P. O (1998) **Isolation and Characterization of Rat Liver Amphisomes: EVIDENCE FOR FUSION OF AUTOPHAGOSOMES WITH BOTH EARLY AND LATE ENDOSOMES*** *Journal of Biological Chemistry* **273**:21883–21892 <https://doi.org/10.1074/jbc.273.34.21883>
- 9 Fader C. M., Sánchez D., Furlán M., Colombo M. I (2008) **Induction of Autophagy Promotes Fusion of Multivesicular Bodies with Autophagic Vacuoles in K562 Cells** *Traffic* **9**:230–250 <https://doi.org/10.1111/j.1600-0854.2007.00677.x>
- 10 Jeppesen D. K., et al. (2019) **Reassessment of Exosome Composition** *Cell* **177**:428–445 <https://doi.org/10.1016/j.cell.2019.02.029>
- 11 Valcz G., et al. (2019) **En bloc release of MVB-like small extracellular vesicle clusters by colorectal carcinoma cells** *Journal of Extracellular Vesicles* **8** <https://doi.org/10.1080/20013078.2019.1596668>
- 12 Mathieu M., et al. (2021) **Specificities of exosome versus small ectosome secretion revealed by live intracellular tracking of CD63 and CD9** *Nature Communications* **12** <https://doi.org/10.1038/s41467-021-24384-2>

- 13 Kovács K. D., et al. (2023) **Nanoinjection of extracellular vesicles to single live cells by robotic fluidic force microscopy** *Journal of Extracellular Vesicles* **12** <https://doi.org/10.1002/jev2.12388>
- 14 Klionsky D. J., et al. (2021) **Guidelines for the use and interpretation of assays for monitoring autophagy (4th edition)**¹ *Autophagy* **17**:1–382 <https://doi.org/10.1080/15548627.2020.1797280>
- 15 Xie D., et al. (2022) **Autophagy Contributes to the Rapamycin-Induced Improvement of Otitis Media** *Frontiers in Cellular Neuroscience* **15**
- 16 Chen P. M., Gombart Z. J., Chen J. W (2011) **Chloroquine treatment of ARPE-19 cells leads to lysosome dilation and intracellular lipid accumulation: possible implications of lysosomal dysfunction in macular degeneration** *Cell Biosci* **1** <https://doi.org/10.1186/2045-3701-1-10>
- 17 Wang R., et al. (2021) **Molecular basis of V-ATPase inhibition by bafilomycin A1** *Nature Communications* **12** <https://doi.org/10.1038/s41467-021-22111-5>
- 18 Edgar J. R., Manna P. T., Nishimura S., Banting G., Robinson M. S (2016) **Tetherin is an exosomal tether** *eLife* **5** <https://doi.org/10.7554/eLife.17180>
- 19 Ortega F. G., et al. (2019) **Interfering with endolysosomal trafficking enhances release of bioactive exosomes** *Nanomedicine: Nanotechnology, Biology and Medicine* **20** <https://doi.org/10.1016/j.nano.2019.102014>
- 20 Zhang Z., et al. (2020) **Rapamycin maintains NAD(+)/NADH redox homeostasis in muscle cells** *Aging (Albany NY)* **12**:17786–17799
- 21 Tanida I., Ueno T., Kominami E (2008) **LC3 and Autophagy** *Methods Mol Biol* **445**:77–88 https://doi.org/10.1007/978-1-59745-157-4_4
- 22 Liang H., et al. **Liang, H. et al. The formation of migrasomes is initiated by the assembly of sphingomyelin synthase 2 foci at the leading edge of migrating cells.**
- 23 Ma L., et al. (2015) **Discovery of the migrasome, an organelle mediating release of cytoplasmic contents during cell migration** *Cell Research* **25**:24–38 <https://doi.org/10.1038/cr.2014.135>
- 24 Baselga M., et al. (2023) **Spheresomes are the main extracellular vesicles in low-grade gliomas** *Scientific Reports* **13** <https://doi.org/10.1038/s41598-023-38084-y>
- 25 Junquera C., et al. (2016) **Biogenesis of a new type of extracellular vesicles in gastrointestinal stromal tumors: ultrastructural profiles of spheresomes** *Histochem Cell Biol* **146**:557–567 <https://doi.org/10.1007/s00418-016-1460-5>
- 26 Petersen J. D., Mekhedov E., Kaur S., Roberts D. D., Zimmerberg J (2023) **Endothelial cells release microvesicles that harbour multivesicular bodies and secrete exosomes** *Journal of Extracellular Biology* **2** <https://doi.org/10.1002/jex2.79>
- 27 Lai C. P., et al. (2015) **Visualization and tracking of tumour extracellular vesicle delivery and RNA translation using multiplexed reporters** *Nature Communications* **6** <https://doi.org/10.1038/ncomms8029>

- 28 Vukman K. V., et al. (2020) **An implanted device enables in vivo monitoring of extracellular vesicle-mediated spread of pro-inflammatory mast cell response in mice** *Journal of Extracellular Vesicles* **10** <https://doi.org/10.1002/jev2.12023>
- 29 Németh K., et al. (2023) **High fat diet and PCSK9 knockout modulates lipid profile of the liver and changes the expression of lipid homeostasis related genes** *Nutrition & Metabolism* **20** <https://doi.org/10.1186/s12986-023-00738-z>
- 30 Németh K., et al. (2021) **Extracellular vesicle release and uptake by the liver under normo- and hyperlipidemia** *Cellular and Molecular Life Sciences* **78**:7589–7604 <https://doi.org/10.1007/s00018-021-03969-6>
- 31 Koncz A., et al. (2023) **Endoplasmic Reticulum Is a Hypoxia-Inducible Endoplasmic Reticulum-Derived Cargo of Extracellular Vesicles Released by Cardiac Cell Lines** *Membranes* **13**
- 32 Olah I., Kendall C., Glick B (1992) **Differentiation of bursal secretory-dendritic cells studied with anti-vimentin monoclonal antibody** *The Anatomical Record* **233**:111–120 <https://doi.org/10.1002/ar.1092330115>
- 33 Koontz L (2014) **TCA precipitation** *Methods Enzymol* **541**:3–10 <https://doi.org/10.1016/b978-0-12-420119-4.00001-x>
- 34 Visnovitz T., Solti Á., Csikós G., Fricke W (2012) **Plasma membrane H⁺-ATPase gene expression, protein level and activity in growing and non-growing regions of barley (*Hordeum vulgare*) leaves** *Physiologia Plantarum* **144**:382–393 <https://doi.org/10.1111/j.1399-3054.2012.01578.x>

Article and author information

Tamás Visnovitz

Semmelweis University, Department of Genetics, Cell- and Immunobiology, Nagyváradi tér 4. 1089 Budapest, Hungary, ELTE Eötvös Loránd University, Department of Plant Physiology and Molecular Plant Biology, Pázmány Péter sétány 1/c, 1117 Budapest, Hungary
For correspondence: visnovitz.tamas@med.semmelweis-univ.hu
 ORCID iD: [0000-0002-7962-5083](https://orcid.org/0000-0002-7962-5083)

Dorina Lenzinger

Semmelweis University, Department of Genetics, Cell- and Immunobiology, Nagyváradi tér 4. 1089 Budapest, Hungary
 ORCID iD: [0000-0003-0270-7985](https://orcid.org/0000-0003-0270-7985)

Anna Koncz

Semmelweis University, Department of Genetics, Cell- and Immunobiology, Nagyváradi tér 4. 1089 Budapest, Hungary, HUN-REN-SU Translational Extracellular Vesicle Research Group, Nagyváradi tér 4. 1089 Budapest, Hungary

Péter M Vizi

Semmelweis University, Department of Genetics, Cell- and Immunobiology, Nagyváradi tér 4. 1089 Budapest, Hungary

Tünde Bárkai

Semmelweis University, Department of Genetics, Cell- and Immunobiology, Nagyváradi tér 4.
1089 Budapest, Hungary

Krisztina V Vukman

Semmelweis University, Department of Genetics, Cell- and Immunobiology, Nagyváradi tér 4.
1089 Budapest, Hungary

Alicia Galinsoga

Semmelweis University, Department of Genetics, Cell- and Immunobiology, Nagyváradi tér 4.
1089 Budapest, Hungary

Krisztina Németh

Semmelweis University, Department of Genetics, Cell- and Immunobiology, Nagyváradi tér 4.
1089 Budapest, Hungary, HUN-REN-SU Translational Extracellular Vesicle Research Group,
Nagyváradi tér 4. 1089 Budapest, Hungary

Kelsey Fletcher

Semmelweis University, Department of Genetics, Cell- and Immunobiology, Nagyváradi tér 4.
1089 Budapest, Hungary

Zsolt I Komlósi

Semmelweis University, Department of Genetics, Cell- and Immunobiology, Nagyváradi tér 4.
1089 Budapest, Hungary

Péter Lőrincz

ELTE Eötvös Loránd University, Department of Anatomy, Cell and Developmental Biology,
Pázmány Péter sétány 1/c, 1117 Budapest, Hungary
ORCID iD: [0000-0001-7374-667X](https://orcid.org/0000-0001-7374-667X)

Gábor Valcz

Semmelweis University, Department of Genetics, Cell- and Immunobiology, Nagyváradi tér 4.
1089 Budapest, Hungary, HUN-REN-SU Translational Extracellular Vesicle Research Group,
Nagyváradi tér 4. 1089 Budapest, Hungary, Department of Image Analysis, 3DHISTECH Ltd,
Budapest, Hungary

Edit I Buzás

Semmelweis University, Department of Genetics, Cell- and Immunobiology, Nagyváradi tér 4.
1089 Budapest, Hungary, HUN-REN-SU Translational Extracellular Vesicle Research Group,
Nagyváradi tér 4. 1089 Budapest, Hungary, HCEMM-SU Extracellular Vesicle Research Group,
Hungary, Nagyváradi tér 4. 1089 Budapest, Hungary

For correspondence: buzas.edit@med.semmelweis-univ.hu

ORCID iD: [0000-0002-3744-206X](https://orcid.org/0000-0002-3744-206X)

Copyright

© 2024, Visnovitz et al.

This article is distributed under the terms of the [Creative Commons Attribution License](https://creativecommons.org/licenses/by/4.0/), which permits unrestricted use and redistribution provided that the original author and source are credited.

Editors

Reviewing Editor

Hugo Bellen

Baylor College of Medicine, Houston, United States of America

Senior Editor

Felix Campelo

Institute of Photonic Sciences, Barcelona, Spain

Reviewer #1 (Public Review):

Summary:

The authors' research group had previously demonstrated the release of large multivesicular body-like structures by human colorectal cancer cells. This manuscript expands on their findings, revealing that this phenomenon is not exclusive to colorectal cancer cells but is also observed in various other cell types, including different cultured cell lines, as well as cells in the mouse kidney and liver. Furthermore, the authors argue that these large multivesicular body-like structures originate from intracellular amphisomes, which they term "amphictosomes." These amphictosomes release their intraluminal vesicles (ILVs) through a "torn-bag mechanism." Finally, the authors demonstrate that the ILVs of amphictosomes are either LC3B positive or CD63 positive. This distinction implies that the ILVs either originate from amphisomes or multivesicular bodies, respectively.

Strengths:

The manuscript reports a potential origin of extracellular vesicle (EV) biogenesis. The reported observations are intriguing.

Weaknesses:

It is essential to note that the manuscript has issues with experimental designs and lacks consistency in the presented data. Here is a list of the major concerns:

- (1) The authors culture the cells in the presence of fetal bovine serum (FBS) in the culture medium. Given that FBS contains a substantial amount of EVs, this raises a significant issue, as it becomes challenging to differentiate between EVs derived from FBS and those released by the cells. This concern extends to all transmission electron microscopy (TEM) images (Figure 1, 2P-S, S5, Figure 4 P-U) and the quantification of EV numbers in Figure 3. The authors need to use an FBS-free cell culture medium.
- (2) The data presented in Figure 2 is not convincingly supportive of the authors' conclusion. The authors argue that "...CD81 was present in the plasma membrane-derived limiting membrane (Figures 2B, D, F), while CD63 was only found inside the MV-IEVs (Fig. 2A, C, E)." However, in Figure 2G, there is an observable CD63 signal in the limiting membrane (overlapping with the green signals), and in Figure 2J, CD81 also exhibits overlap with MV-IEVs.
- (3) Following up on the previous concern, the authors argue that CD81 and CD63 are exclusively located on the limiting membrane and MV-IEVs, respectively (Figure 2-A-M). However, in lines 104-106, the authors conclude that "The simultaneous presence of CD63, CD81, TSG101, ALIX, and the autophagosome marker LC3B within the MV-IEVs..." This statement indicates that CD63 and CD81 co-localize to the MV-IEVs. The authors need to address this apparent discrepancy and provide an explanation.

(4) The specificity of the antibodies used in Figure 2 should be validated through knockout or knockdown experiments. Several of the antibodies used in this figure detect multiple bands on western blots, raising doubts about their specificity. Verification through additional experimental approaches is essential to ensure the reliability and accuracy of all the immunostaining data in this manuscript.

(5) In Figures 2P-R, the morphology of the MV-IEVs does not resemble those shown in Figures 1-A, H, and D, indicating a notable inconsistency in the data.

(6) There are no loading controls provided for any of the western blot data. Additionally, for Figures 2-S4B, the authors should run the samples from lanes i-iii in a single gel.

(7) In Figure 2-S4, is there co-localization observed between LC3RFP (LC3A?) with other MV-IFV markers? How about LC3B? Does LC3B co-localize with other MV-IFV markers?

(8) The TEM images presented in Figure 2-S5, specifically F, G, H, and I, do not closely resemble the images in Figure 2-S5 K, L, M, N, and O. Despite this dissimilarity, the authors argue that these images depict the same structures. The authors should provide an explanation for this observed discrepancy to ensure clarity and consistency in the interpretation of the presented data.

(9) For Figures 3C and 3-S1, the authors should include the images used for EV quantification. Considering the concern regarding potential contamination introduced by FBS (concern 1), it is advisable for the authors to employ an independent method to identify EVs, thereby confirming the reliability of the data presented in these figures.

(10) Do the amphiectosomes released from other cell types as well as cells in mouse kidneys or liver contain LC3B positive and CD63 positive ILVs?

<https://doi.org/10.7554/eLife.95828.1.sa2>

Reviewer #2 (Public Review):

Summary:

The authors had previously identified that a colorectal cancer cell line generates small extracellular vesicles (sEVs) via a mechanism where a larger intracellular compartment containing these sEVs is secreted from the surface of the cell and then tears to release its contents. Previous studies have suggested that intraluminal vesicles (ILVs) inside endosomal multivesicular bodies and amphisomes can be secreted by the fusion of the compartment with the plasma membrane. The 'torn bag mechanism' considered in this manuscript is distinctly different because it involves initial budding off of a plasma membrane-enclosed compartment (called the amphiectosome in this manuscript, or MV-IEV). The authors successfully set out to investigate whether this mechanism is common to many cell types and to determine some of the subcellular processes involved.

The strengths of the study are:

(1) The high-quality imaging approaches used, seem to show good examples of the proposed mechanism.

(2) They screen several cell lines for these structures, also search for similar structures in vivo, and show the tearing process by real-time imaging.

(3) Regarding the intracellular mechanisms of ILV production, the authors also try to demonstrate the different stages of amphiectosome production and differently labelled ILVs

using immuno-EM.

Several of these techniques are technically challenging to do well, and so these are critical strengths of the manuscript.

The weaknesses are:

(1) Most of the analysis is undertaken with cell lines. In fact, all of the analysis involving the assessment of specific proteins associated with amphiectosomes and ILVs are performed in vitro, so it is unclear whether these processes are really mirrored in vivo. The images shown in vivo only demonstrate putative amphiectosomes in the circulation, which is perhaps surprising if they normally have a short half-life and would need to pass through an endothelium to reach the vessel lumen unless they were secreted by the endothelial cells themselves.

(2) The analysis of the intracellular formation of compartments involved in the secretion process (Figure 2_S5) relies on immuno-EM, which is generally less convincing than high-/super-resolution fluorescence microscopy because the immuno-labelling is inevitably very sporadic and patchy. High-quality EM is challenging for many labs (and seems to be done very well here), but high-/super-resolution fluorescence microscopy techniques are more commonly employed, and the study already shows that these techniques should be applicable to studying the intracellular trafficking processes.

(3) One aspect of the mechanism, which needs some consideration, is what happens to the amphisome membrane, once it has budded off inside the amphiectosome. In the fluorescence images, it seems to be disrupted, but presumably, this must happen after separation from the cell to avoid the release of ILVs inside the cell. There is an additional part of Figure 1 (Figure 1Y onwards), which does not seem to be discussed in the text (and should be), that alludes to amphiectosomes often having a double membrane.

(4) The real-time analysis of the amphiectosome tearing mechanism seemed relatively slow to me (over three minutes), and if this has been observed multiple times, it would be helpful to know if this is typical or whether there is considerable variation.

Overall, I think the authors have been successful in identifying amphiectosomes secreted from multiple cell lines and demonstrating that the ILVs inside them have at least two origins (autophagosome membrane and late endosomal multivesicular body) based on the markers that they carry. The analysis of intracellular compartments producing these structures is rather less convincing and it remains unclear what cells release these structures in vivo.

I think there could be a significant impact on the EV field and consequently on our understanding of cell-cell signalling based on these findings. It will flag the importance of investigating the release of amphiectosomes in other studies, and although the authors do not discuss it, the molecular mechanisms involved in this type of 'ectosomal-style' release will be different from multivesicular compartment fusion to the plasma membrane and should be possible to be manipulated independently. Any experiments that demonstrate this would greatly strengthen the manuscript.

In general, the EV field has struggled to link up analysis of the subcellular biology of sEV secretion and the biochemical/physical analysis of the sEVs themselves, so from that perspective, the manuscript provides a novel angle on this problem.

<https://doi.org/10.7554/eLife.95828.1.sa1>

Reviewer #3 (Public Review):

Summary:

In this manuscript, the authors describe a novel mode of release of small extracellular vesicles. These small EVs are released via the rupture of the membrane of so-called amphiectosomes that resemble "morphologically" Multivesicular Bodies.

These structures have been initially described by the authors as released by colorectal cancer cells (<https://doi.org/10.1080/20013078.2019.1596668>). In this manuscript, they provide experiments that allow us to generalize this process to other cells. In brief, amphiectosomes are likely released by ectocytosis of amphisomes that are formed by the fusion of multivesicular endosomes with autophagosomes. The authors propose that their model puts forward the hypothesis that LC3 positive vesicles are formed by "curling" of the autophagosomal membrane which then gives rise to an organelle where both CD63 and LC3 positive small EVs co-exist and would be released then by a budding mechanism at the cell surface that appears similar to the budding of microvesicles /ectosomes. Very correctly the authors make the distinction from migrasomes because these structures appear very similar in morphology.

Strengths:

The findings are interesting despite that it is unclear what would be the functional relevance of such a process and even how it could be induced. It points to a novel mode of release of extracellular vesicles.

Weaknesses:

This reviewer has comments and concerns concerning the interpretation of the data and the proposed model. In addition, in my opinion, some of the results in particular micrographs and immunoblots (even shown as supplementary data) are not of quality to support the conclusions.

<https://doi.org/10.7554/eLife.95828.1.sa0>

Author Response

eLife assessment

The authors present evidence that small extracellular vesicles can be secreted from cells inside larger vesicles that they call amphiectosomes, which then tear to release their small vesicle contents. There are questions and concerns relating to the quality of the data and the in vivo significance of the observations. The findings are potentially important but the data are incomplete and the claims are only partially supported.

We agree that the in vivo significance and details of the molecular background of amphiectosome release remains to be studied further. However, as Reviewer 2 indicated, our data in this Short Report may have a substantial impact on our understanding of EV biogenesis. Therefore, we considered it was important to publish our data as soon as possible because it may significantly impact other EV biogenesis studies.

Public Reviews:

Reviewer #1 (Public Review):

Summary:

The authors' research group had previously demonstrated the release of large multivesicular body-like structures by human colorectal cancer cells. This manuscript

expands on their findings, revealing that this phenomenon is not exclusive to colorectal cancer cells but is also observed in various other cell types, including different cultured cell lines, as well as cells in the mouse kidney and liver. Furthermore, the authors argue that these large multivesicular body-like structures originate from intracellular amphisomes, which they term "amphictosomes." These amphictosomes release their intraluminal vesicles (ILVs) through a "torn-bag mechanism." Finally, the authors demonstrate that the ILVs of amphictosomes are either LC3B positive or CD63 positive. This distinction implies that the ILVs either originate from amphisomes or multivesicular bodies, respectively.

Strengths:

The manuscript reports a potential origin of extracellular vesicle (EV) biogenesis. The reported observations are intriguing.

Weaknesses:

It is essential to note that the manuscript has issues with experimental designs and lacks consistency in the presented data. Here is a list of the major concerns:

(1) The authors culture the cells in the presence of fetal bovine serum (FBS) in the culture medium. Given that FBS contains a substantial amount of EVs, this raises a significant issue, as it becomes challenging to differentiate between EVs derived from FBS and those released by the cells. This concern extends to all transmission electron microscopy (TEM) images (Figure 1, 2P-S, S5, Figure 4 P-U) and the quantification of EV numbers in Figure 3. The authors need to use an FBS-free cell culture medium.

(1) Although FBS indeed contains bovine EVs, however, the presence of very large multivesicular EVs (amphictosomes) that our manuscript focuses on has never been observed and reported. For reported size distributions of EVs in FBS, please find a few relevant references below:

PMID: 29410778, PMID: 33532042, PMID: 30940830 and PMID: 37298194

All the above publications show that the number of IEVs > 350-500 nm is negligible in FBS. The average diameter of MV-IEVs (amphictosomes) described in our manuscript is around 1.00-1.50 micrometre.

(1) When we demonstrated the TEM of isolated EVs, we consistently used serum- free conditioned medium (Fig2 P-S, Fig2S5 J, O) as described previously (Németh et al 2021, PMID: 34665280).

(2) Our TEM images show cells captured in the process of budding and scission of large multivesicular EVs excluding the possibility that these structures could have originated from FBS.

(3) In addition, in our confocal analysis, we studied Palm-GFP positive, cell-line derived MV-IEVs. Importantly, in these experiments, FBS-derived EVs are non-fluorescent, therefore, the distinction between GFP positive MV-IEVs and FBS-derived EVs was evident.

(4) In addition, culturing cells in FBS-free medium (serum starvation) significantly affects autophagy. Given that in our study, we focused on autophagy related amphictosome secretion, we intentionally chose to use FBS supplemented medium.

(5) Even though the authors of this manuscript are not familiar with the technological details how FBS is processed before commercialization, it is reasonable to assume that the samples are subjected to sterile filtration (through a 0.22 micron filter) after which MV-IEVs cannot be present in the commercial FBS samples.

(2) The data presented in Figure 2 is not convincingly supportive of the authors' conclusion. The authors argue that "...CD81 was present in the plasma membrane-derived limiting membrane (Figures 2B, D, F), while CD63 was only found inside the MV-IEVs (Fig. 2A, C, E)." However, in Figure 2G, there is an observable CD63 signal in the limiting membrane (overlapping with the green signals), and in Figure 2J, CD81 also exhibits overlap with MV-IEVs.

Both CD63 and CD81 are tetraspanins known to be present both in the membrane of sEVs and in the plasma membrane of cells (for references, please see Uniprot subcellular location maps: https://www.uniprot.org/uniprotkb/P08962/entry#subcellular_location https://www.uniprot.org/uniprotkb/P60033/entry#subcellular_location). However, according the feedback of the reviewer, for clarity, we will delete the implicated sentence from the text.

(3) Following up on the previous concern, the authors argue that CD81 and CD63 are exclusively located on the limiting membrane and MV-IEVs, respectively (Figure 2-A-M). However, in lines 104-106, the authors conclude that "The simultaneous presence of CD63, CD81, TSG101, ALIX, and the autophagosome marker LC3B within the MV-IEVs..." This statement indicates that CD63 and CD81 co-localize to the MV-IEVs. The authors need to address this apparent discrepancy and provide an explanation.

There must be a misunderstanding because we did not claim or implicate in the text that that "CD81 and CD63 are exclusively located on the limiting membrane and MV-IEVs". Here we studied co-localization of the above proteins in the case intraluminal vesicles (ILVs). In Fig 2. we did not show any analysis of limiting membrane co-localization.

(4) The specificity of the antibodies used in Figure 2 should be validated through knockout or knockdown experiments. Several of the antibodies used in this figure detect multiple bands on western blots, raising doubts about their specificity. Verification through additional experimental approaches is essential to ensure the reliability and accuracy of all the immunostaining data in this manuscript.

We will consider this suggestion during the revision of the manuscript.

(5) In Figures 2P-R, the morphology of the MV-IEVs does not resemble those shown in Figures 1-A, H, and D, indicating a notable inconsistency in the data.

EM images in Figure2 P-R show sEVs separated from serum-free conditioned media as opposed to MV-IEVs, which were in situ captured in in fixed tissue cultures (Fig1). Therefore, the two EV populations necessarily have different size and structure. Furthermore, Fig. 1 shows images of ultrathin sections while in Figure 2P-R, we used a negative-positive contrasting of intact sEV-s without embedding and sectioning.

(6) There are no loading controls provided for any of the western blot data.

Not even the latest MISEV 2023 guidelines give recommendations for proper loading control for separated EVs in Western blot (MISEV 2023 , DOI: 10.1002/jev2.12404 PMID: 38326288). Here we applied our previously developed method (PMID: 37103858), which in our opinion, is the most reliable approach to be used for sEV Western blotting. For whole cell lysates, we used actin as loading control (Fig3_S2B).

Additionally, for Figures 2-S4B, the authors should run the samples from lanes i-iii in a single gel.

Please note that in Figure 2- S4B, we did run a single gel, and the blot was cut into 4 pieces, which were tested by anti-GFP, anti-RFP, anti-LC3A and anti-LC3B antibodies. Full Western blots are shown in Fig.3_S2 B, and lanes “1”, “2” and “3” correspond to “i”, “ii” and “iii” in Fig.2_S4, respectively.

(7) In Figure 2-S4, is there co-localization observed between LC3RFP (LC3A?) with other MV-IFV markers? How about LC3B? Does LC3B co-localize with other MV-IFV markers?

In the Supplementary figure Figure 2-S4 we showed successful generation of HEK293T-PalmGFP-LC3RFP cell line. In this case we tested the cells, and not the released MV-IEVs. LC3A co-localized with the RFP signal as expected.

(8) The TEM images presented in Figure 2-S5, specifically F, G, H, and I, do not closely resemble the images in Figure 2-S5 K, L, M, N, and O. Despite this dissimilarity, the authors argue that these images depict the same structures. The authors should provide an explanation for this observed discrepancy to ensure clarity and consistency in the interpretation of the presented data.

As indicated in Material and Methods, Fig 2_S5 F, G, H and I are conventional TEM images fixed by 4% glutaraldehyde 1% OsO₄ 2h and embedded into Epon resin with a post contrasting of 3.75% uranyl acetate 10 min and 12 min lead citrate. Samples processed this way have very high structure preservation and better image quality, however, they are not suitable for immune detection. In contrast, Fig.2_S5 K,L,M,N shows immunogold labelling of in situ fixed samples. In this case we used milder fixation (4% PFA, 0.1% glutaraldehyde, postfixed by 0.5% OsO₄ 30 min) and LR-White hydrophilic resin embedding. This special resin enables immunogold TEM analysis. The sections were exposed to H₂O₂ and NaBH₄ to render the epitopes accessible in the resin. Because of the different applied techniques, the preservation of the structure is not the same. In the case of Fig.2 J, O, separated sEVs were visualised by negative-positive contrast and immunogold labelling as described previously (PMID: 37103858).

(9) For Figures 3C and 3-S1, the authors should include the images used for EV quantification. Considering the concern regarding potential contamination introduced by FBS (concern 1), it is advisable for the authors to employ an independent method to identify EVs, thereby confirming the reliability of the data presented in these figures.

In our revised manuscript, we will provide all the images used for EV quantification in Figure 3C. Given that Figures 3C and 3-S1 show MV-IEVs released by HEK293T-PlamGFP cells, the possible interference by FBS-derived non-fluorescent EVs can be excluded.

(10) Do the amphiectosomes released from other cell types as well as cells in mouse kidneys or liver contain LC3B positive and CD63 positive ILVs?

Based on our confocal microscopic analysis, in addition the HEK293T-PalmGFP cells, HT29 and HepG2 cells also release similar LC3B and CD63 positive MV-IEVs. Preliminary evidence shows MV-IEV secretion by additional cell types.